nature communications

Article

https://doi.org/10.1038/s41467-025-66974-4

Autoantibody landscape and functional role of anti-C-C motif chemokine receptor 8 autoantibodies in systemic sclerosis: post-hoc analysis of a B-cell depletion trial

Received: 5 August 2024

Accepted: 20 November 2025

Kazuki M. Matsuda[1,6], Yang-Yi Chen[2,6], Satoshi Ebata[1], Kazuhiro Iwadoh[1], Hirohito Kotani[1], Ai Kuzumi[1], Asako Yoshizaki-Ogawa[1], Cheng-Che E. Lan[2,3], Hsin-Su Yu[2], Hayakazu Sumida[1,4,5] & Shinichi Sato[1]

Systemic sclerosis (SSc) is an autoimmune disease marked by fibrosis and extensive autoantibody production. Although B-cell depletion with rituximab (RTX) has shown clinical benefit, predictive biomarkers of response remain elusive. Here, we apply proteome-wide autoantibody screening using wet protein arrays covering 13,455 human antigens in serum samples from participants of the randomized trial of RTX. We identify a significant elevation in the total autoantibody levels in SSc compared to healthy controls, with greater reductions post-treatment observed in RTX high responders than in low responders. A stepwise selection highlights 88 clinically relevant autoantibodies, including those targeting G protein-coupled receptors. Among them, anti-C-C motif chemokine receptor 8 (CCR8) autoantibodies are functionally validated by cell-based assays using CCR8-overexpressing HEK293 cells. Furthermore, in a bleomycin-induced mouse model, anti-CCR8 antibody administration exacerbates dermal fibrosis and modifies immune cell infiltration. Although external validation with multiple comparison adjustment is further required, these findings reveal an autoantibody signature associated with therapeutic response and pathogenic potential in SSc, providing a foundation for precision immunotherapy and mechanistic insights into disease progression.

Systemic sclerosis (SSc) is a progressive fibrotic autoimmune disease that affects the skin and various internal organs[1]. Among connective tissue diseases, SSc carries the worst prognosis, with an estimated 10-year mortality rate of approximately 30%[2]. Although dermal fibrosis—quantified by the modified Rodnan skin score (mRSS)—serves as a clinical marker of disease severity[3], it is increasingly recognized that preceding immune dysregulation plays a pivotal role in disease initiation and progression. In particular, abnormalities in B cells[4–6], as well as in regulatory T cells (Tregs)[7–9], contribute to a dysregulated immune environment that promotes chronic inflammation and fibroblast activation. Such an inflammation-to-fibrosis axis is a central pathogenic feature of SSc[10].

---

[1]Department of Dermatology, The University of Tokyo Hospital, Tokyo, Japan. [2]Department of Dermatology, Kaohsiung Medical University Hospital, Kaohsiung Medical University, Kaohsiung, Taiwan. [3]Biomedical Artificial Intelligence Academy, Kaohsiung Medical University, Kaohsiung, Taiwan. [4]Scleroderma Center, The University of Tokyo Hospital, Tokyo, Japan. [5]SLE Center, The University of Tokyo Hospital, Tokyo, Japan. [6]These authors contributed equally: Kazuki M. Matsuda, Yang-Yi Chen. e-mail: matsudak-der@h.u-tokyo.ac.jp; satos-der@h.u-tokyo.ac.jp

Reflecting this evolving understanding, several therapeutic strategies targeting B cells have emerged, including monoclonal antibodies[11–13], Bruton's tyrosine kinase inhibitors[14–16], and chimeric antigen receptor (CAR) T-cell therapies[17–19]. These approaches aim not only to suppress autoantibody production, but also to mitigate the pro-inflammatory and pro-fibrotic functions of B cells and their crosstalk with other immune cells[20]. Moreover, autologous Treg infusion has recently demonstrated promising results in SSc[21].

Rituximab (RTX) is a chimeric monoclonal antibody (Ab) that depletes circulating B cells by targeting the B-cell-specific antigen CD20. Previously, we conducted a double-blind, investigator-initiated, randomized, placebo-controlled trial, or the DESIRES trial[14], which demonstrated significant superiority of RTX over placebo by the absolute reduction of mRSS 24 weeks after initiation of the study period. The open-label extension of this trial further revealed the long-term efficacy and safety of RTX on SSc[22], as well as the association between decrease in serum immunoglobulins and greater clinical response to RTX[23]. Although previous studies identified several factors associated with treatment response to RTX in SSc[24,25], reliably stratifying RTX-responsive patients remains a significant challenge—particularly given the potential risks associated with long-term immunosuppression. It is also noteworthy that RTX treatment ameliorates abnormal Treg skewing, although the disease context differs from SSc and the underlying mechanisms remain unclear[26,27].

The emergence of autoantibodies is a prominent feature of SSc, highlighting its nature as an autoimmune disorder. Anti-nuclear antibodies (ANAs), detected through indirect immunofluorescence on HEp-2 cells, are present in more than 90% of patients with SSc[28]. Several ANAs are specific to SSc or are closely associated with distinct clinical subsets. For instance, anti-topoisomerase I antibodies (ATA) are strongly linked to diffuse skin sclerosis and severe interstitial lung disease (ILD), while anti-centromere antibodies (ACA) are primarily associated with limited skin and lung involvement[29]. However, the pathogenicity of these ANAs is debated, as they cannot reach their targets across the plasma and nuclear membranes in vivo. Additionally, the DESIRES trials revealed that serum ATA levels did not decrease[22,30], indicating that the relationship between serum immunoglobulin levels and responsiveness to RTX cannot be explained by ATA levels.

Our group has developed an original platform for proteome-wide autoantibody screening (PWAbS) using wet protein arrays (WPAs), enabling high-throughput, quantitative measurement of more than ten thousand human antigens[31,32]. This technique has previously been used to develop multiplex measurements for disease-related autoantibodies[33,34], identify clinically relevant novel autoantibodies[35–37], and investigate inter- and intra-molecular epitope spreading during the disease course[38].

In this study, we apply this original PWAbS platform to comprehensively characterize the autoantibody landscape of SSc and its modulation by rituximab therapy. We identify a subset of autoantibodies associated with therapeutic response and highlight anti-chemokine receptor 8 (CCR8) autoantibodies with functional and pathogenic significance. These findings delineate dynamic immunological changes following B-cell depletion and uncover novel mechanisms linking autoreactivity to fibrosis, providing a foundation for precision immunotherapy in SSc and insights into its pathophysiology.

Results

Subjects

In the DESIRES trial (NCT04274257), a total of 56 individuals diagnosed with SSc were evenly randomized into two groups: 28 received RTX and 28 received a placebo[30]. Serum samples were collected at the start and after 24 weeks of treatment from participants who completed the term. These samples were reacted with WPAs for PWAS (Fig. 1A). After excluding samples that were not suitable for PWAbS, such as those containing anti-GST-tag antibodies, the study proceeded with 24 patients in the RTX group and 21 patients in the placebo group. The baseline characteristics of the two groups were comparable (Table 1). An equal number of age- and sex-matched healthy controls (HCs; $n = 45$) were also included in the study (Fig. 1B).

The sum of autoantibody levels

First, we validated our autoantibody measurements by comparing serum levels of well-established SSc-related autoantibodies—ATA, ACA, and anti-RNA polymerase III (ARA)—obtained using clinical-standard ELISAs with those generated by our PWAbS platform. The results demonstrated strong positive correlations between the two methods (Fig. 1C).

Next, we defined the sum of autoantibody levels (SAL) as the total serum concentration of all autoantibodies assessed in our PWAbS. SAL was significantly higher in SSc patients compared to HCs at the baseline ($P < 0.0001$; Fig. 2A). Subsequently, we categorized the RTX treatment group into two subgroups based on their response in skin sclerosis to treatment (Fig. 2B): high responders (HRs; $n = 11$) and low responders (LRs; $n = 13$). Initially, SAL was significantly greater in the HR group compared to the LR group ($P < 0.05$; Fig. 2C). Additionally, SAL levels decreased significantly from week 0 to week 24 in the HR group ($P < 0.05$), whereas changes in the LR group were not statistically significant. This pattern persisted across all age groups (Supplementary Fig. 1A). In contrast, serum levels of well-known SSc-related autoantibodies, including ATA, ACA, and ARA, did not follow this trend, as observed both in clinical-standard ELISA tests (Fig. 2D) and in our PWAbS (Supplementary Fig. 1B).

Machine learning

To determine which autoantibodies were driving the association between the SAL and disease status, we first utilized nine machine learning frameworks. Notably, Lasso regression, Ridge regression, SVM with normalization, XGBoost, and LightGBM achieved an area under the receiver-operator characteristics curve (ROC-AUC) exceeding 0.96, demonstrating an almost perfect ability to distinguish between SSc patients and HCs (Supplementary Table 1). We identified the top 10 features in these six models (Supplementary Fig. 2A), examined their inclusion relationships (Supplementary Fig. 2B), and explored the prevalence of highlighted autoantibodies across a broader range of human disorders using the aUToAntiBody Comprehensive Database (UT-ABCD)[39]. Most of these autoantibodies were found to be non-specifically elevated in various pathological conditions, except for well-known SSc-specific autoantibodies such as ATA and ARA (Supplementary Fig. 2C). Attempts to distinguish between HRs and LRs based on pre-treatment autoantibody profiles did not yield satisfactory precision (Supplementary Table 1).

Investigating clinically relevant autoantibodies

We next sought to identify autoantibodies significantly associated with the clinical features of SSc using the trial data that included longitudinal changes. Initially, we selected autoantibodies that were significantly elevated in SSc patients compared to HCs at baseline (Fig. 3A and Supplementary Data 1). Next, we chose autoantibodies that were significantly higher in HRs compared to LRs (Fig. 3B and Supplementary Data 2). Lastly, we focused on autoantibodies whose serum concentrations significantly decreased from week 0 to week 24 in HRs (Fig. 3C and Supplementary Data 3). As a result, 88 autoantibodies were identified as candidates for clinically relevant autoantibodies in SSc (Fig. 3D). Principal component analysis (PCA) indicated that these 88 autoantibodies appear to distinguish HRs at week 0 within the dataset, especially by negative values of the principal component 1 (Fig. 3E). Autoantibodies targeting G protein-coupled receptors (GPCRs) contributed to negative values of the principal component 1

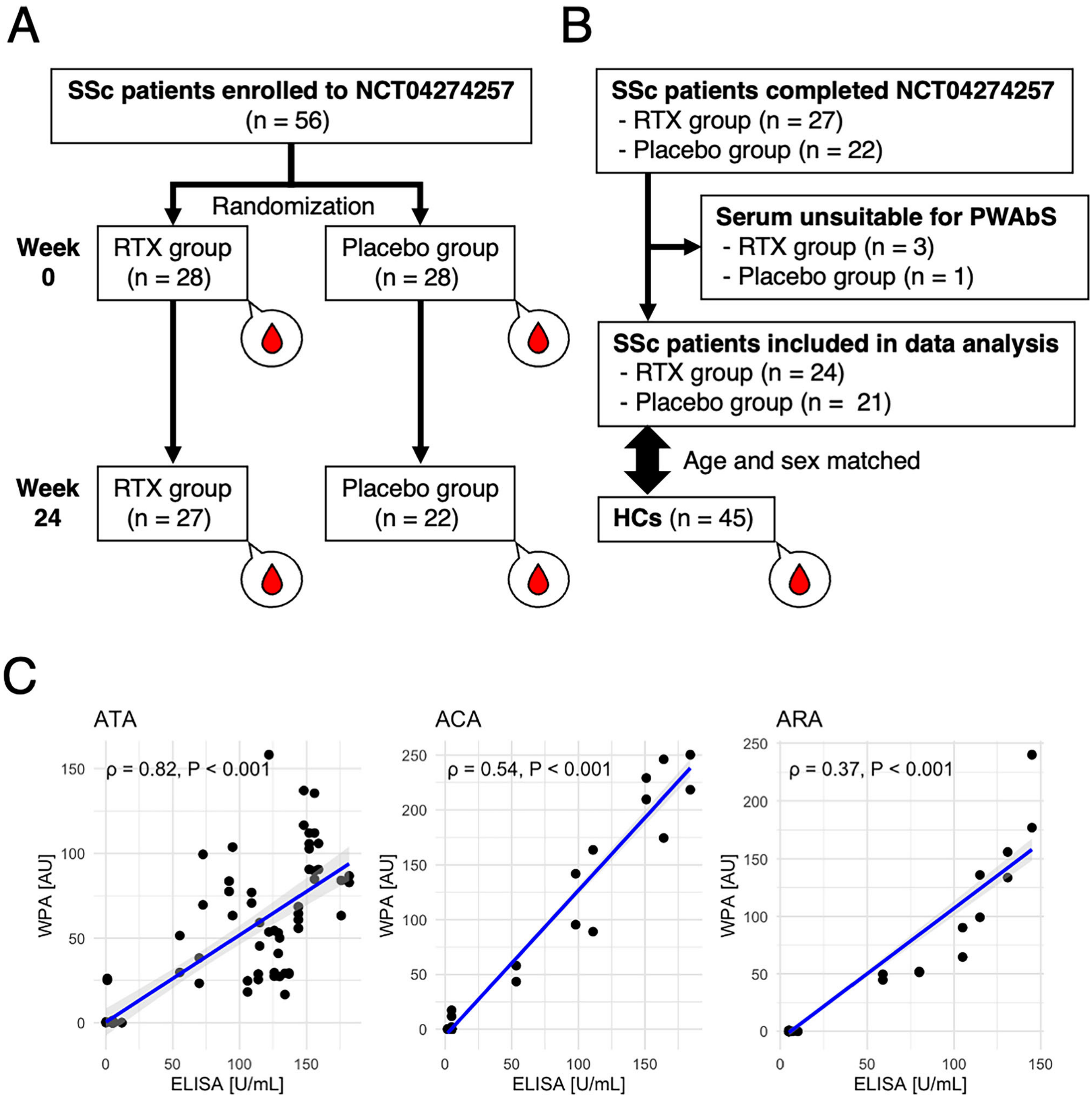

Fig. 1 | Overview of the study. A The study design of the DESIRES trial. **B** The flow chart of sample acquisition in the present study. Age and sex-matched healthy controls (HCs) were recruited. Source data are provided as a Source Data file. **C** Scatter plots illustrate the correlation between serum levels of anti-topoisomerase I antibody (ATA), anti-centromere antibody (ACA), and anti-RNA polymerase III antibody (ARA) measured by enzyme-linked immunosorbent assays (ELISA) and WPAs. Each dot represents an individual patient. Blue lines indicate linear regression fits with 95% confidence intervals (shaded area). Spearman's correlation coefficient (ρ) and associated P-values are shown in each panel.

(Fig. 3F). We also identified autoantibodies significantly increased in SSc compared to healthy controls after correction for multiple comparisons (Supplementary Data 4), among which all these autoantibodies targeting GPCRs remained statistically significant.

Profiling candidate autoantibodies

The GPCRs targeted by autoantibodies included C-C motif chemokine receptor 8 (CCR8), neuropeptide FF receptor 2 (NPFFR2), P2Y receptor family member 8 (P2RY8), melanocortin 1 receptor (MC1R), 5-hydroxytryptamine receptor 1B (HTR1B), and formyl peptide receptor 1 (FPR1). Their serum levels are illustrated in Fig. 4A. The associations between each autoantibody and the clinical characteristics of SSc are detailed in Fig. 4B and Supplementary Fig. 3A, which highlighted a positive correlation between anti-CCR8 autoantibody levels and mRSS, the primary endpoint of the DESIRES trial. The serum levels of anti-CCR8 autoantibodies were also significantly correlated with Health Assessment Questionnaire Disability Index (HAQ-DI) scores. We also investigated the distribution of these highlighted autoantibodies in a broader population, utilizing UT-ABCD. As a result, the median and the maximum of serum levels of anti-CCR8 autoantibody was the highest in SSc, compared to coronavirus infection 2019 (COVID-19), atopic dermatitis (AD), anti-neutrophil cytoplasmic antibody-associated vasculitis (AAV), systemic lupus erythematosus (SLE), and HCs (Supplementary Fig. 3B).

Table 1 | Baseline characteristics of the human subjects

	SSc on RTX ($n=24$)	SSc on placebo ($n=21$)	HC ($n=45$)
Basic features			
Sex			
Female	22 (91.7%)	19 (90.5%)	41 (91.1%)
Male	2 (8.3%)	2 (9.5%)	4 (8.9%)
Age, years	48.79 (15.50)	49.24 (9.66)	44.09 (14.05)
Disease duration, months	96.75 (73.75)	77.29 (64.69)	NA
mRSS	13.58 (3.26)	15.67 (5.43)	NA
ILD presence	24 (100.0%)	19 (90.5%)	NA
ILD severity	1.25 (0.44)	1.05 (0.50)	NA
Pulmonary function			
%FVC	87.42 (15.91)	90.19 (18.61)	NA
%DLco	84.55 (19.63)	83.12 (14.56)	NA
Laboratory tests			
SP-A, ng/mL	40.81 (25.81)	43.45 (29.76)	NA
SP-D, ng/mL	153.11 (80.93)	165.99 (133.82)	NA
KL-6, U/mL	771.42 (759.63)	667.10 (720.64)	NA
BNP, ng/mL	32.71 (58.86)	23.33 (13.92)	NA
IgA, mg/mL	205.29 (65.69)	229.81 (85.52)	NA
IgG, mg/mL	1349.12 (371.67)	1421.71 (548.83)	NA
IgM, mg/mL	127.75 (44.68)	94.52 (39.89)	NA
Seum autoantibody levels			
ATA, U/mL	80.24 (65.11)	69.91 (67.25)	NA
ACA, U/mL	22.75 (49.80)	19.08 (40.08)	NA
ARA, U/mL	20 ± 37	17 ± 37	NA
RNP, U/mL	20.26 (36.67)	16.63 (36.60)	NA
SF-36 score			
Bodily pain	62.67 (26.35)	58.48 (24.37)	NA
General health	46.71 (14.01)	46.14 (14.87)	NA
Mental health	70.00 (19.45)	70.24 (19.40)	NA
Physical functioning	80.83 (15.99)	75.71 (15.83)	NA
Role, emotional	80.90 (25.83)	79.76 (28.33)	NA
Role, physical	69.79 (25.65)	71.43 (21.34)	NA
Social functioning	79.17 (26.50)	81.55 (15.11)	NA
Vaitality	48.44 (25.29)	51.49 (15.55)	NA
HAQ-DI score			
total	0.32 (0.48)	0.45 (0.41)	NA
HAQ1 (dressing and grooming)	0.29 (0.62)	0.38 (0.50)	NA
HAQ2 (arising)	0.04 (0.20)	0.19 (0.40)	NA
HAQ3 (eating)	0.58 (0.93)	0.90 (0.89)	NA
HAQ4 (walking)	0.04 (0.20)	0.24 (0.44)	NA
HAQ5 (hygiene)	0.12 (0.34)	0.19 (0.40)	NA
HAQ6 (reach)	0.38 (0.71)	0.43 (0.68)	NA
HAQ7 (grip)	0.62 (0.82)	0.71 (0.64)	NA
HAQ8 (common daily activities)	0.38 (0.82)	0.52 (0.81)	NA

Data are n (%), mean (SD), or median (range). *SSc* systemic sclerosis, *RTX* rituximab, *HC* healthy control, *mRSS* modified Rodnan skin score,*ILD* interstitial lung disease, *% FVC* percent predicted forced vital capacity, *%DLco* percent predicted diffusing capacity for carbon monoxide, *KL-6* sialylated carbohydrate antigen Krebs von den Lungen-6, *SP-A* surfactant protein-A,*SP-D* surfactant protein-D, *BNP* brain natriuretic peptide, *ATA* anti-topoisomerase antibody, *ACA* anti-centromere antibody,*ARA* anti-RNA polymerase III antibody, *RNP* anti-ribonucleoprotein antibody, *SF-36* 36-item short-form general health survey, *HAQ-DI* health assessment questionnaire disability index.

Weighted correlation network analysis

We utilized weighted correlated network analysis (WGCNA)[40] to delve deeper into the correlations between autoantibodies in SSc. Our analysis included 135 specimens from SSc patients at week 0 ($n=45$) and week 24 ($n=45$), as well as HCs ($n=45$). We constructed a correlation network for all autoantibodies evaluated in our PWAbS and identified 57 distinct modules (Fig. 5A). The "turquoise" module contained ATA, as well as anti-CCR8, anti-MC1R, and anti-P2RY8 autoantibodies (Supplementary Data 5). The "darkmagenta" module, which included ARA, and the "tan" module, which included ACA, did not contain any of the GPCR-targeting autoantibodies highlighted above. We reviewed the associations between each module and clinical traits (Fig. 5B). The "turquoise" module was positively linked to ATA, a higher mRSS – the primary endpoint of the DESIRES trial – as well as to lower patient-reported quality of life, evidenced by higher HAQ-DI scores and lower 36-Item Short Form Health Survey (SF-36) scores. The "darkmagenta" module was associated with ARA positivity and higher forced vital capacity of the lungs, indicating a lower degree of ILD. The "tan" module was correlated with the ACA profile but did not show any significant associations with other clinical traits

Validation of anti-CCR8 antibody by cell-based assay

Before proceeding with functional analyses, we first confirmed the presence of anti-CCR8 autoantibodies in patient sera using a cell-based assay. Plasmids encoding *CCR8* gene were constructed (Supplementary Fig. 4A and Supplementary Data 6) and transfected into HEK293 cells. RT-qPCR confirmed robust overexpression of *CCR8* in the transduced cells compared to wild-type controls (fold change > 60,000-fold). Surface expression of CCR8 was further verified by immunocytochemistry (Supplementary Fig. 4B) and flow cytometry (Supplementary Fig. 4C). Using these CCR8-overexpressing cells, we performed flow cytometry with IgG fractions purified from anti-CCR8-positive SSc sera and anti-CCR8-negative healthy HC sera, with or without preincubation with an anti-CCR8 monoclonal Ab. Mean fluorescence intensity (MFI), detected by a fluorophore-conjugated anti-human IgG Fc secondary Ab, was significantly higher in cells treated with anti-CCR8-positive IgG compared to controls, and this signal was attenuated by CCR8 blockade (Fig. 6A, B). No such difference was observed in non-transfected HEK293 cells (Supplementary Fig. 4D, E).

ERK phosphorylation assay

Next, we examined whether anti-CCR8 autoantibodies in SSc sera function as agonists or antagonists of CCR8 signaling. CCR8-overexpressing HEK293 cells were incubated with chemokine ligand 1 (CCL1), the physiological agonist of CCR8, in the presence of either anti-CCR8-positive IgG or control IgG. Phosphorylation levels of ERK, a downstream effector of CCR8 signaling[41,42], were quantified using an enzyme-linked immunosorbent assay (ELISA). Co-stimulation with anti-CCR8–positive IgG reduced ERK phosphorylation compared with CCL1 stimulation alone, whereas co-stimulation with control IgG did not produce a significant change (Fig. 6C), indicating that anti-CCR8 autoantibodies exert an antagonistic effect on CCR8 signaling in SSc.

Treg migration assay

The tissue specificity of CCR8 was investigated using publicly available databases. Analysis of multiple human tissues through bulk RNA sequencing data from the Human Protein Atlas[43] revealed that *CCR8* are enriched in bone marrow and lymphoid tissues. Single-cell RNA sequencing data from the Tabula Sapiens project[44] showed that *CCR8* expression is enhanced in a subset of Tregs. Based on these findings, we focused on Tregs as the primary cellular target of anti-CCR8 autoantibodies. To evaluate the functional impact of these autoantibodies, we conducted Treg migration assays using dual-chamber culture systems. Tregs were collected from the peripheral blood of a

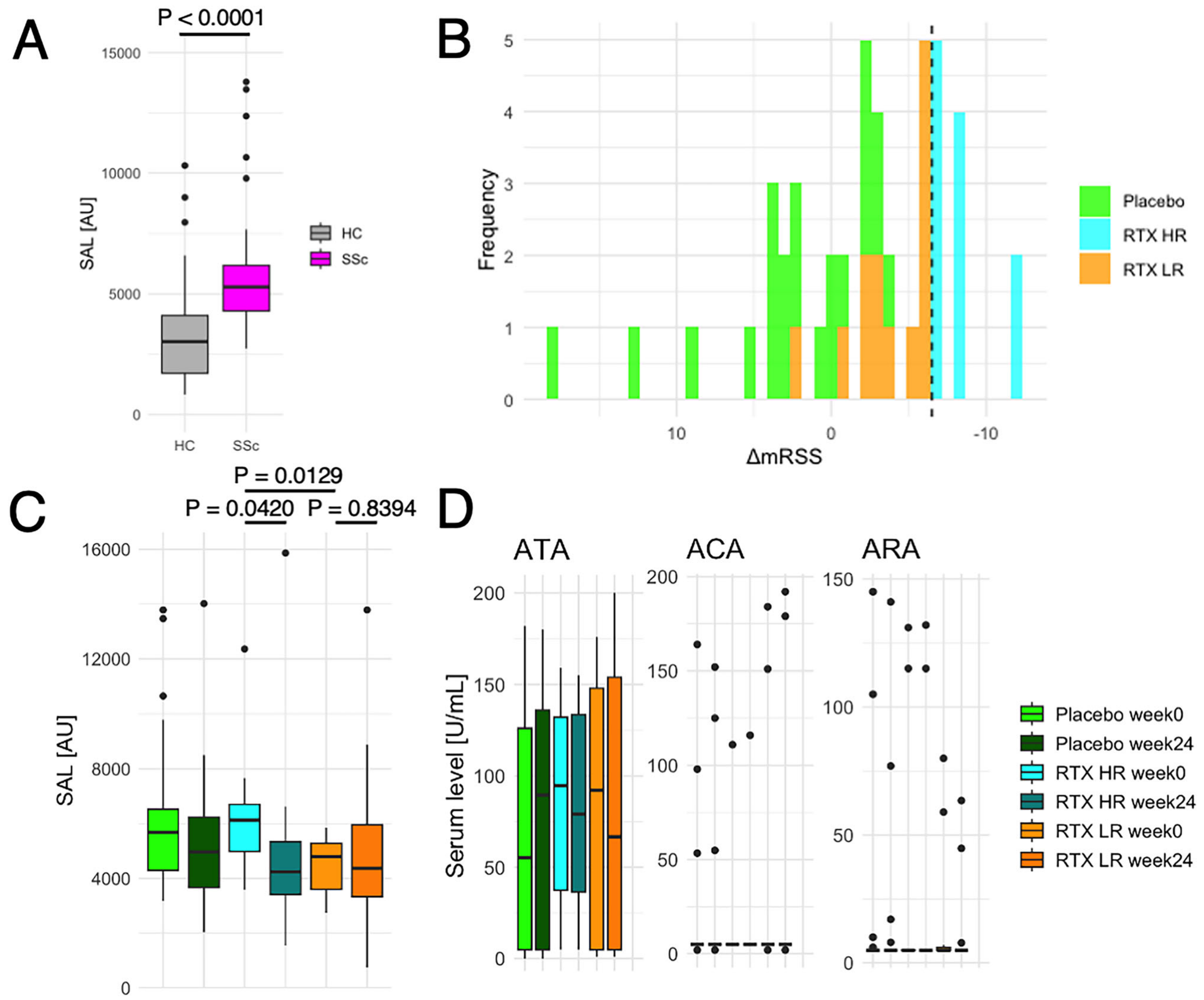

Fig. 2 | Sum of autoantibody levels. **A** The sum of autoantibody levels (SAL) in systemic sclerosis (SSc; *n* = 45) at the baseline and healthy controls (HCs; *n* = 45). P values were calculated by two-sided Mann-Whitney's U test. **B** Absolute change of mRSS in SSc patients during the DESIREs trial before and after rituximab (RTX) or placebo administration (week 0 and week 24). HR: high responder, LR: low responder. **C** SAL before and after the study period of the DESIRES trial by the treatment arm (placebo week 0: *n* = 21, placebo week 24: *n* = 21, RTX HR week 0: *n* = 11, RTX HR week 24: *n* = 11, RTX LR week 0: *n* = 13, RTX LR week 24: *n* = 13). P values were calculated by two-sided Mann–Whitney's U test. **D** Serum levels of SSc-related autoantibodies before and after the study period of the DESIRES trial by the treatment arm (placebo week 0: *n* = 21, placebo week 24: *n* = 21, RTX HR week 0: *n* = 11, RTX HR week 24: *n* = 11, RTX LR week 0: *n* = 13, RTX LR week 24: *n* = 13). ATA anti-topoisomerase I antibody, ACA anti-centromere antibody, ARA anti-RNA polymerase III antibody.

healthy control. Anti-CCR8-positive IgG, but not control IgG, significantly inhibited CCL1-induced Treg migration (Fig. 6D). These results suggest that anti-CCR8 autoantibodies may impair Treg homing from the circulation to the skin, thereby contributing to the exacerbation of skin inflammation in SSc.

Bleomycin-induced mice model

To evaluate the in vivo effects of anti-CCR8 Ab treatment, we employed a bleomycin (BLM)-induced mouse model of skin sclerosis (Fig. 7A). C57BL/6NcrSlc mice were administered daily subcutaneous injections of BLM or phosphate-buffered saline (PBS) as a control for two weeks. On Day 8, a single intraperitoneal injection of either control IgG or anti-CCR8 monoclonal Ab was administered. Skin samples were collected at Day 14 for histological and transcriptomic analyses. Histological examination revealed significantly increased dermal thickness (Fig. 7B, C, D) and decreased number of Tregs infiltrated in the skin in the BLM + anti-CCR8 Ab group relative to the BLM + control IgG group (Fig. 7E and Supplementary Fig. 5).

To assess molecular changes associated with anti-CCR8 Ab treatment, we performed bulk RNA sequencing of PBS or BLM-treated skin samples. Comparative analysis using volcano plots showed substantial transcriptomic alterations in both BLM-treated groups relative to PBS controls (Fig. 8A). Venn diagram analysis identified both shared and unique DEGs between the BLM + control IgG and BLM + anti-CCR8 Ab conditions (Fig. 8B). Unsupervised clustering based on differentially expressed genes (DEGs) revealed distinct transcriptional profiles across the PBS, BLM + control IgG, and BLM + anti-CCR8 Ab groups (Fig. 8C). Gene Ontology (GO) analyses indicated that the BLM + anti-CCR8 Ab group exhibited enrichment of biological processes (BPs) associated with skin development and cytoskeletal contractile organization (Fig. 8D), as well as molecular functions (MFs) involving extracellular matrix (ECM)-associated activities and GPCR binding. Gene Set Enrichment Analysis (GSEA) further revealed significant upregulation of inflammation-related pathways (Fig. 9A). Notably, Ingenuity Pathway Analysis (IPA) predicted activation of bio-functions related to immune-cell migration and infiltration specifically in the

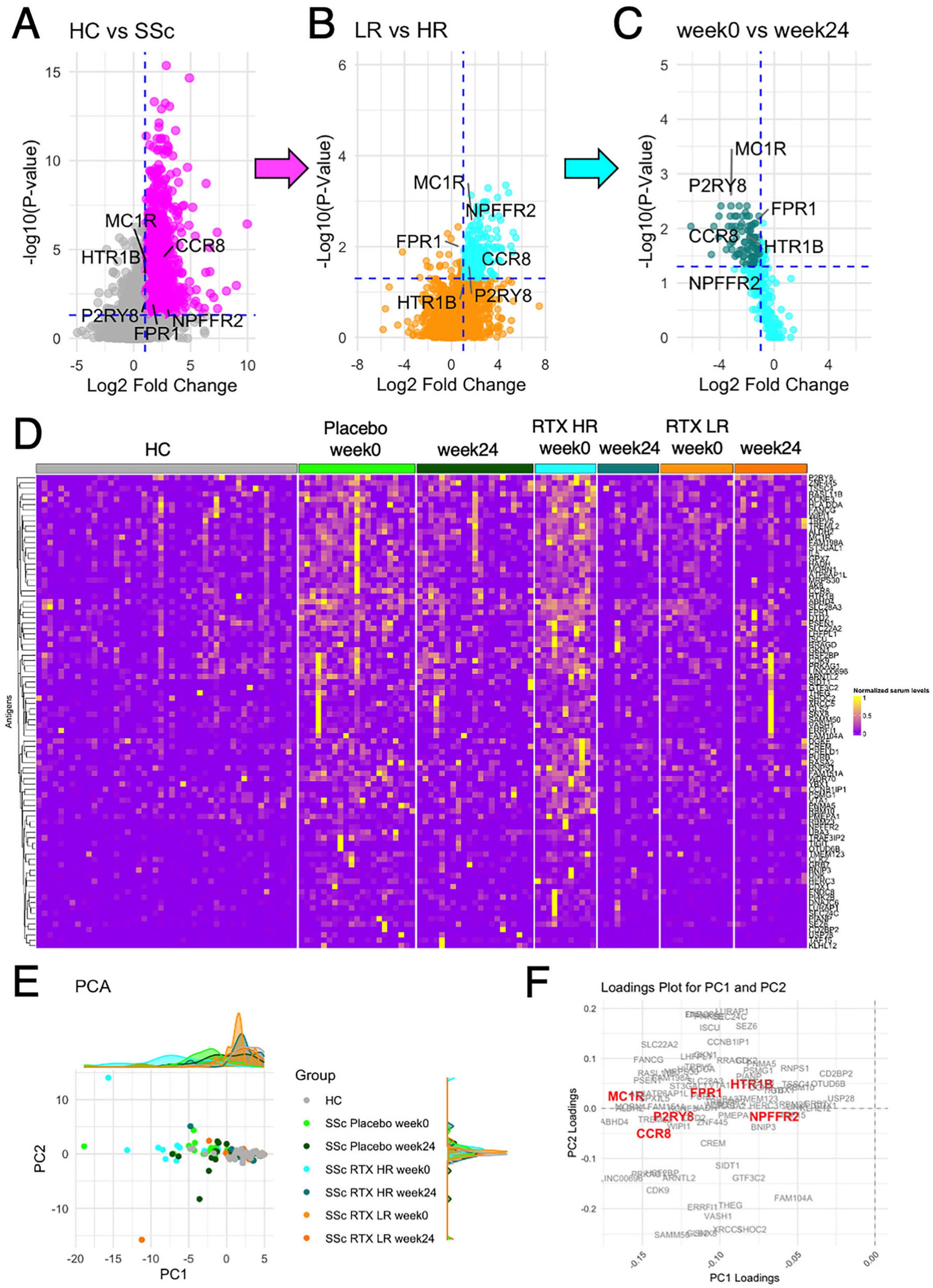

Fig. 3 | Selection of autoantibodies of clinical relevance. **A** Volcano plot that shows autoantibodies differentially elevated in SSc before treatment compared to healthy controls (HCs). The horisontal dashed line indicates *P* = 0.05. **B** Volcano plot that shows autoantibodies differentially increased in HRs than in LRs. **C** Volcano plot that shows autoantibodies significantly reduced in HRs during RTX therapy. **D** Heat map that shows the serum levels of 58 candidate autoantibodies of clinical relevance. **E** Principal component analysis of 58 candidate autoantibodies of clinical relevance. In the scatter plot, individual subjects as points. **F** The loading diagram illustrates the contributions to PC1 and PC2.

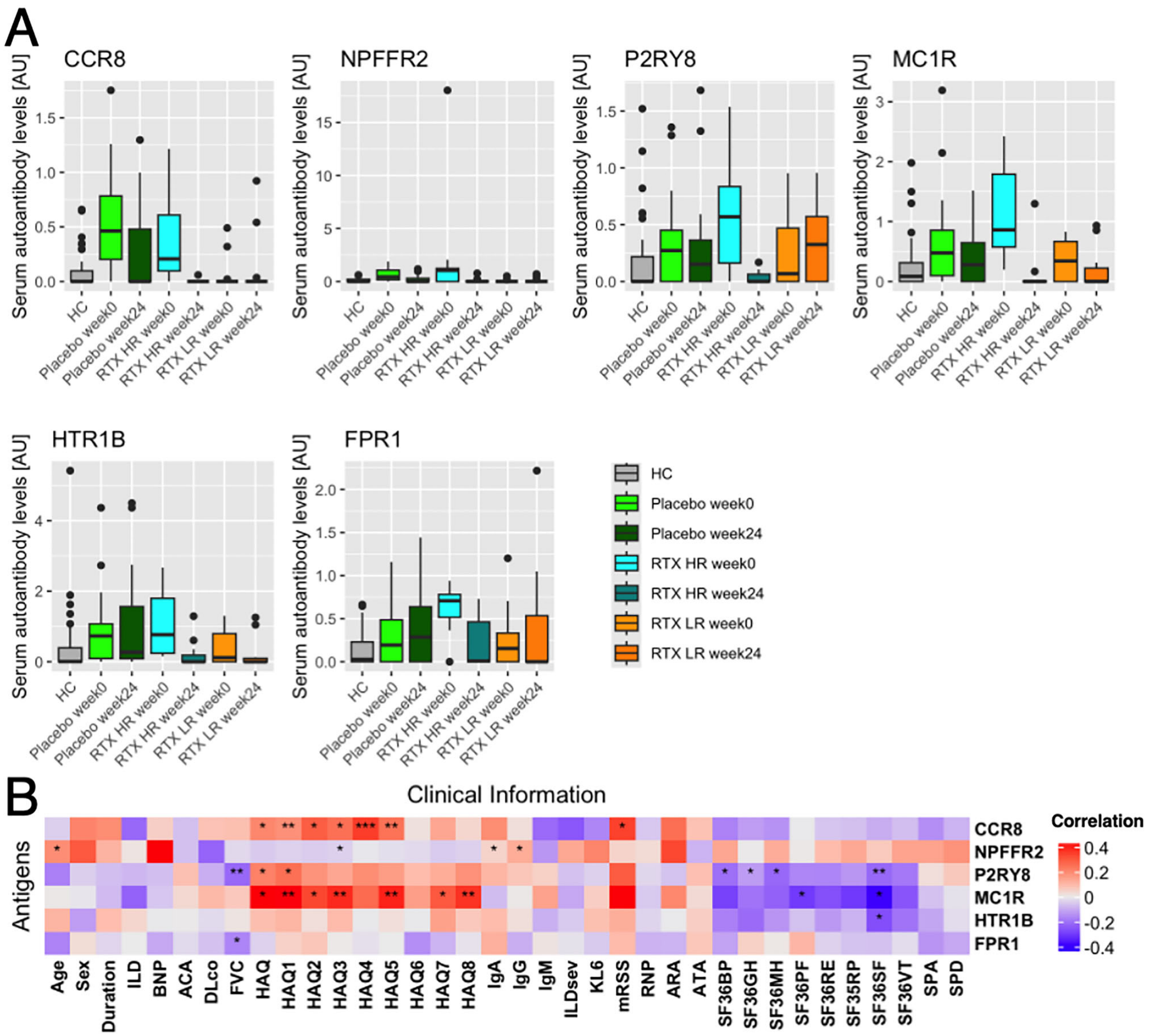

Fig. 4 | Autoantibodies targeting G protein-coupled receptors. **A** Serum levels of autoantibodies targeting G protein-coupled receptors (GPCRs) of clinical relevance by treatment arm (HC: $n = 45$, placebo week 0: $n = 21$, placebo week 24: $n = 21$, RTX HR week 0: $n = 11$, RTX HR week 24: $n = 11$, RTX LR week 0: $n = 13$, RTX LR week 24: $n = 13$). **B** The heatmap illustrates correlation between the autoantibodies targeting GPCRs and clinical traits of SSc. *: $P < 0.05$, **: $P < 0.01$, ***: $P < 0.001$. P values were calculated by Spearman's correlation test.

BLM + anti-CCR8 Ab group (Fig. 9B). In addition, disease categories such as "fibrosis" and "fibrotic disorder of skin" showed higher enrichement in the BLM + anti-CCR8 Ab group compared to BLM + control IgG, suggesting that anti-CCR8 Ab treatment potentiated fibrotic responses in this model (Fig. 9C).

Discussion

In this study, we applied our original PWAbS platform to serum samples from patients with SSc enrolled in the DESIRES trial (Fig. 1), alongside age- and sex-matched HCs. We observed a global increase in circulating autoantibody levels in SSc compared to HCs (Fig. 2). Among these, 88 autoantibodies were identified as clinically relevant candidates, based on their elevation in HRs and decrease following RTX therapy (Fig. 3A–D). PCA revealed partial separation of HRs from LRs (Fig. 3E), where autoantibodies targeting GPCRs contributed prominently to this separation (Fig. 3F), suggesting a link between GPCR-directed immune responses and RTX responsiveness. Among the anti-GPCR autoantibodies (Fig. 4A), serum levels of anti-CCR8 antibodies significantly correlated with mRSS and HAQ scores (Fig. 4B), further supporting their clinical relevance in SSc. These autoantibodies largely clustered into a single module in WGCNA that was associated with ATA positivity, higher mRSS, and lower patient-reported quality of life (Fig. 5A, B).

Our machine learning analysis confirmed that classical SSc-specific antinuclear antibodies, such as ATA and ARA, were among the most powerful discriminators of SSc versus HCs (Supplementary Fig. 2). However, these autoantibodies remained unchanged during RTX treatment (Fig. 2D and Supplementary Fig. 1B) and did not differ between HRs and LRs, limiting their utility as markers of treatment response. This stability likely reflects their origin from long-lived plasma cells, which are not targeted by anti-CD20-mediated B-cell depletion. This interpretation aligns with prior studies showing that ANA titers are generally unaffected by RTX but may decrease in response to therapies that eliminate long-lived plasma cells, such as CAR-T cell therapies[18,22,30]. These observations also underscore a critical limitation of baseline-only models to predict RTX-responsiveness.

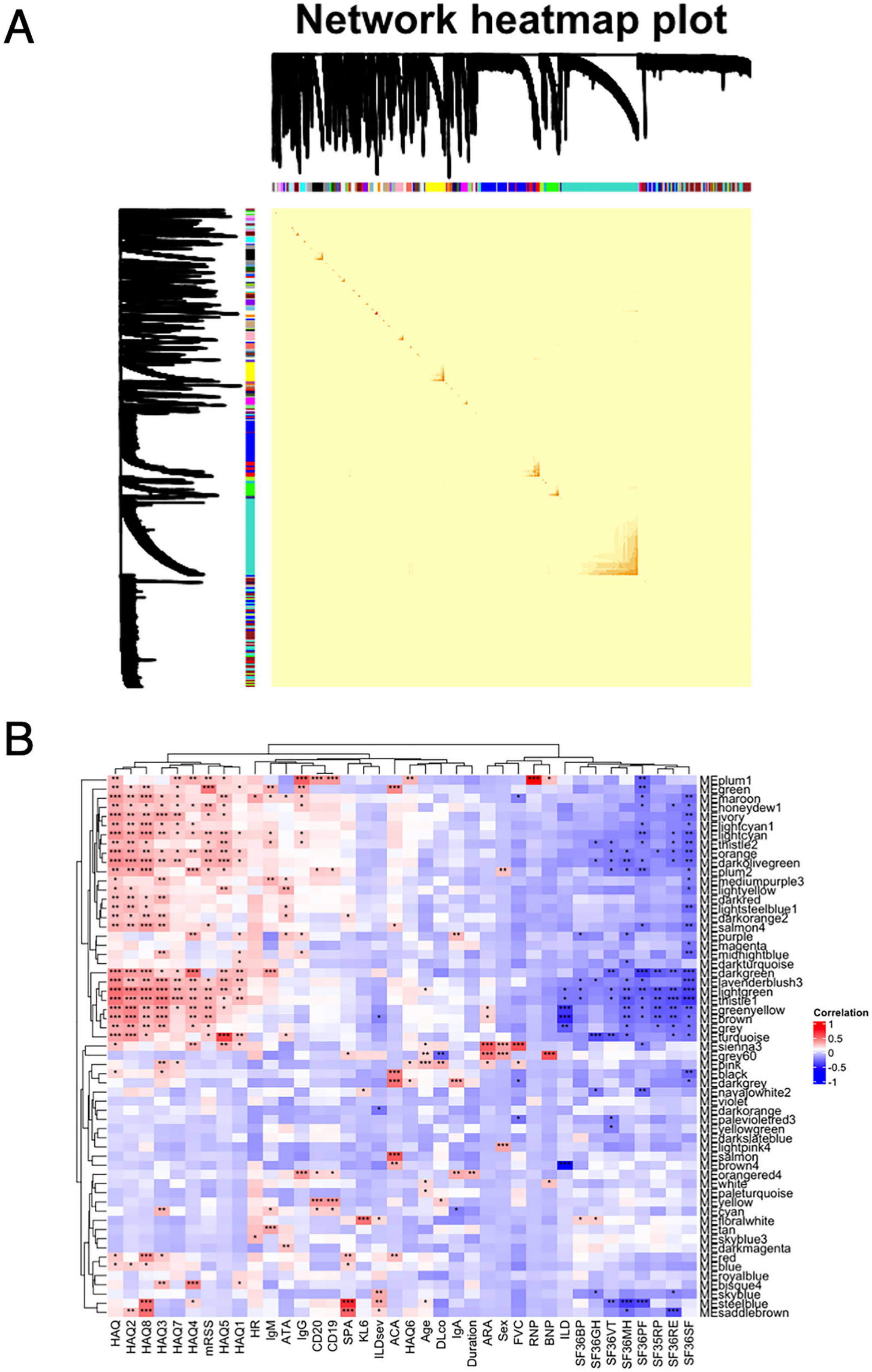

Fig. 5 | Weighted correlation network analysis. **A** Network heatmap plot illustrated by weighted correlation network analysis (WGCNA) analysis. Branches in the hierarchical clustering dendrograms correspond to modules. Color-coded module membership is displayed in the color bars below and to the right of the dendrograms. In the heatmap, high co-expression interconnectedness is indicated by progressively more saturated yellow and red colors. **B** The heatmap shows the correlation between each module and clinical trait. HAQ: health-associated quality of life. HR: high responder. SF36: short-form 36-item health survey. PF: physical functioning. RP: role physical. BP bodily pain. GH: general health. VT: vitality. SF: social functioning. RE: role emotional. MH: mental health. RNP: anti-ribonucleoprotein antibody. *: $P < 0.05$, **: $P < 0.01$, ***: $P < 0.001$. P values were calculated by Spearman's correlation test.

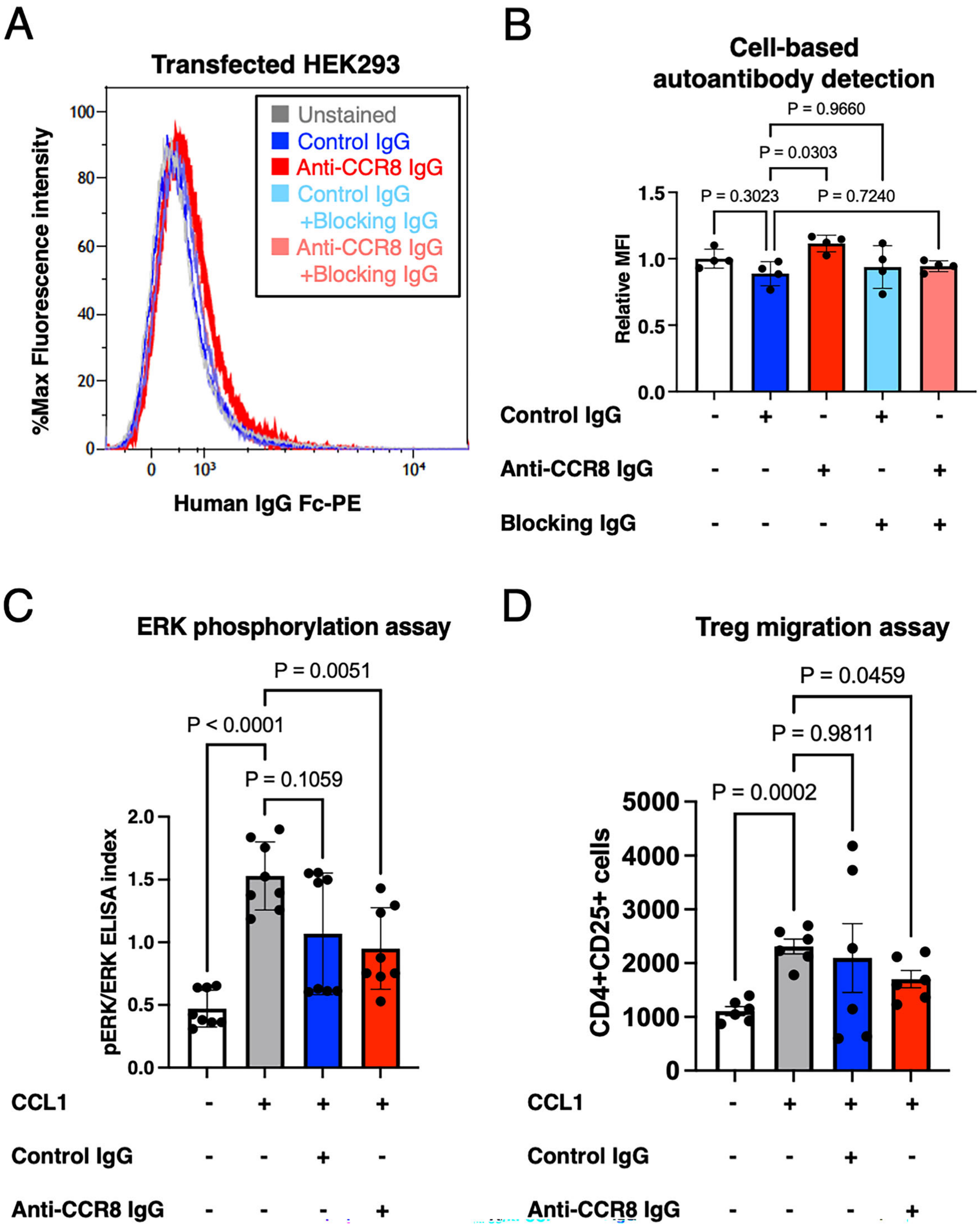

Fig. 6 | Cell-based assays for detection and functional characterization of anti-C-C motif chemokine receptor 8 autoantibodies. A Representative histograms from flow cytometry showing binding of anti-C-C motif chemokine receptor 8 (CCR8)-positive IgG from systemic sclerosis (SSc) patients or healthy controls (HC) to CCR8-overexpressing HEK293 cells. A fluorophore-conjugated anti-human IgG Fc antibody was used for detection. **B** Quantification of mean fluorescence intensity (MFI) in CCR8-overexpressing cells incubated with anti-CCR8-positive or control IgG, with or without preincubation with blocking anti-CCR8 monoclonal antibody (*n* = 4 technical replicates per group). **C** ERK phosphorylation levels in CCR8-overexpressing HEK293 cells after stimulation with CCL1 in the presence of anti-CCR8-positive or control IgG, as measured by ELISA (*n* = 8 biological replicates per group). **D** Treg migration assay in Transwell culture systems. The number of migrated Tregs in response to CCL1 with anti-CCR8-positive IgG or control IgG (*n* = 6 biological replicates per group) are presented. Statistical significance was assessed using Welch's ANOVA with Dunnett's T3 multiple comparison adjustment. Error bars are defined as the standard error of the mean. Source data are provided as a Source Data file.

Our machine learning model did not successfully differentiate HRs from LRs based solely on pretreatment profiles. We propose that this limitation stems from the exclusion of longitudinal immunological dynamics, which, as our data show, are more closely tied to clinical outcomes.

In contrast to the stable SSc-related ANA landscape, we observed dynamic changes in a broader array of non-canonical autoantibodies during RTX therapy, with overall reductions in total autoantibody signal correlating with clinical improvement (Fig. 2A, C). These temporal patterns suggest that short-lived, RTX-sensitive B-lineage cells,

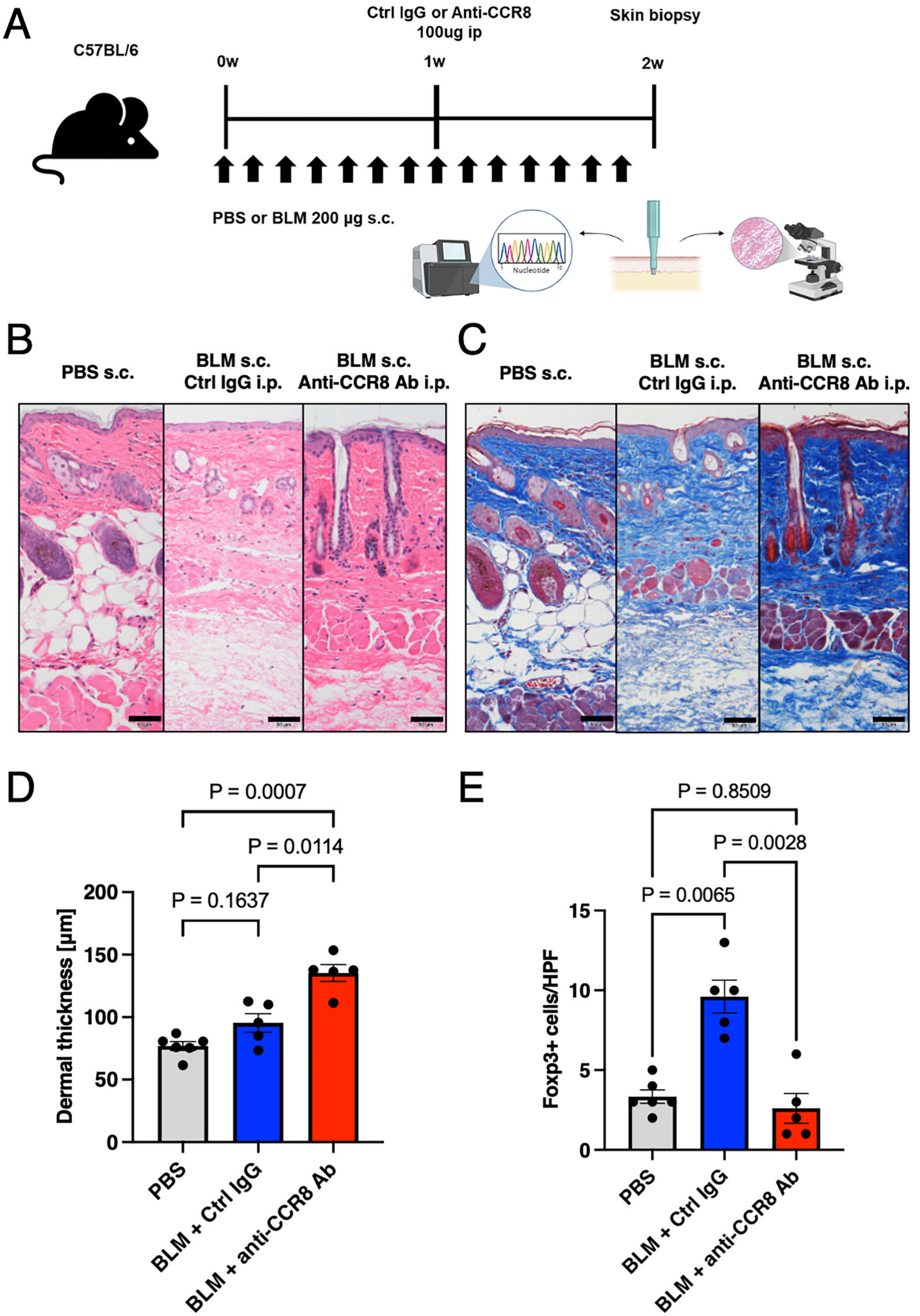

such as plasmablasts, may actively contribute to the evolving autoimmune response. Among these modulated antibodies, we identified a subset with functional relevance—anti-CCR8 Abs—that not only stratified clinical response but also demonstrated biological activity in independent assays. Using a cell-based assay, we confirmed the presence of anti-CCR8 autoantibodies in SSc sera (Fig. 6A, B). Functional assays revealed that these autoantibodies antagonized CCL1-induced ERK phosphorylation (Fig. 6C), and impaired CCL1-driven Treg migration in vitro (Fig. 6D). These findings indicate that anti-CCR8 autoantibodies functionally interfere with Treg chemotaxis, potentially exacerbating tissue inflammation. In a BLM-induced mouse model of skin sclerosis, anti-CCR8 Ab administration aggravated dermal fibrosis (Fig. 7), accompanied by transcriptomic signatures of enhanced inflammation and immune cell trafficking (Figs. 8 and 9).

Fig. 7 | Effect of anti-C-C motif chemokine receptor 8 treatment in a bleomycin-induced systemic sclerosis mouse model. A Experimental protocol of the skin sclerosis mouse model. Six-week-old female C57BL/6NcrSlc mice (MGI ID: MGI:5295404) received daily subcutaneous injections of bleomycin (BLM, 200 μg) or PBS as a control for two weeks. Mice were also treated intraperitoneally with either control (Ctrl) IgG or anti-C-C motif chemokine receptor 8 (CCR8) antibody (Ab) once on Day 8. Skin biopsies were collected at Week 2 for histological analysis and next-generation sequencing (NGS). This figure was partially created with BioRender (https://BioRender.com/slxff50). Representative histological images and quantitative analyses of dermal fibrosis and Treg infiltration in mouse skin. H&E-stained **B** and Masson's trichrome–stained **C** skin sections show increased dermal thickness and collagen deposition following BLM treatment. Images were captured at ×200 magnification, and scale bars represent 50 µm. **D** Quantification of dermal thickness and **E** Foxp3$^+$ Treg counts are presented in the accompanying bar graphs ($n = 6$ biological replicates for PBS group; $n = 5$ biological replicates for BLM-treated groups). Statistical significance was assessed using Welch's ANOVA with Dunnett's T3 multiple comparison adjustment. Error bars are defined as the standard error of the mean. Source data are provided as a Source Data file.

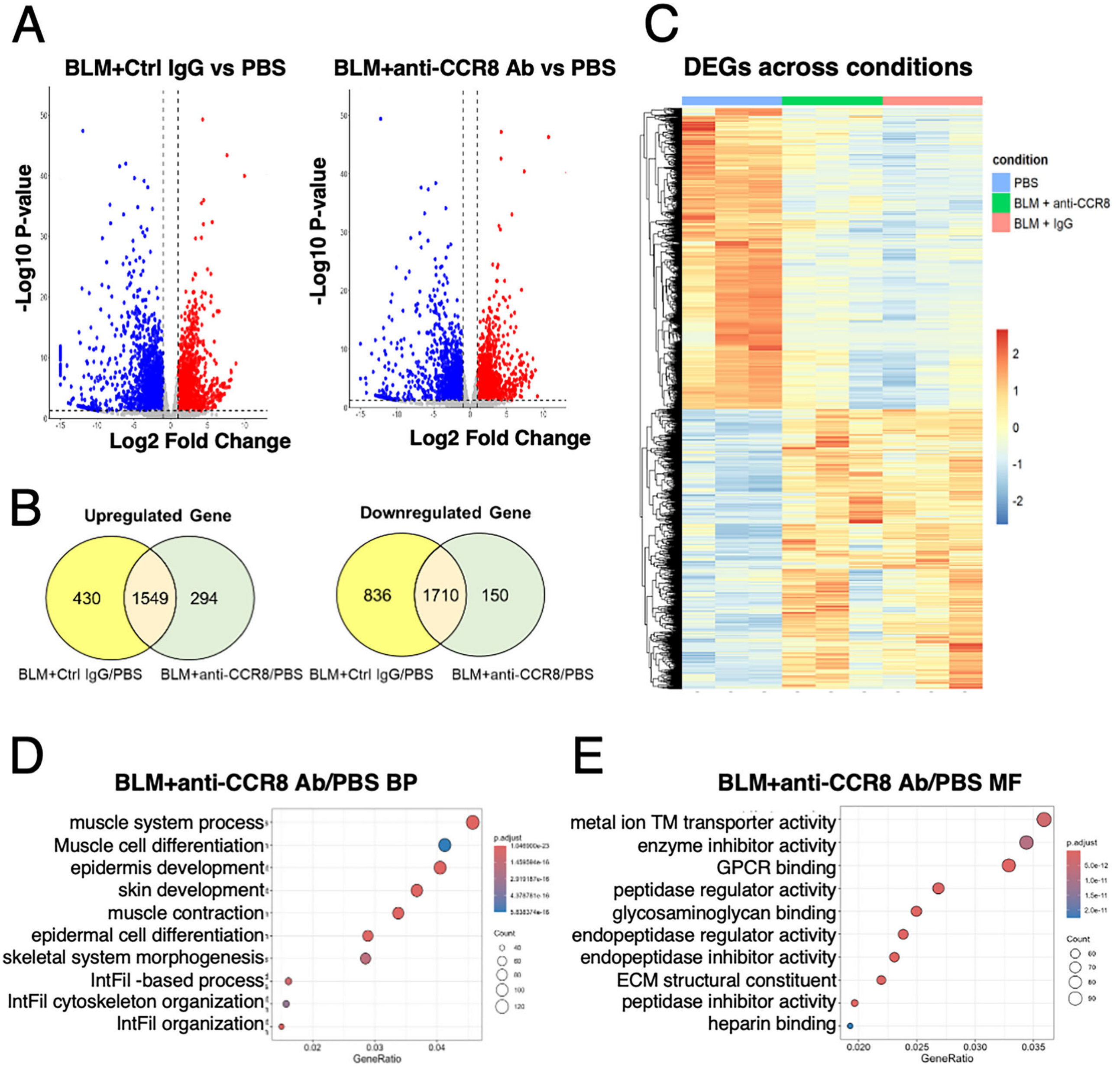

Fig. 8 | Transcriptomic analysis of bleomycin-induced systemic sclerosis mouse model. A Volcano plots show differentially expressed genes (DEGs) in bleomycin (BLM) + control (Ctrl) IgG vs. phosphate buffer saline (PBS) and BLM +anti-C-C motif chemokine receptor 8 (CCR8) antibody (Ab) vs. PBS. Genes are plotted by $\log_2$ fold change and adjusted p-values, with significance thresholds set at adjusted $P < 0.05$ and $|\log_2 \text{ fold change}| > 1.0$. **B** Venn diagrams show overlapping and unique DEGs between comparisons. **C** Heatmap of DEGs identified by NGS, illustrating distinct gene expression profiles among PBS, BLM + Ctrl IgG, and BLM + anti-CCR8 Ab groups. Lower panels display the top 10 enriched **D** biological processes (BPs) and **E** molecular functions (MFs) in the BLM + anti-CCR8 Ab vs. PBS group. Circle size indicates gene count; color represents adjusted p-value. IntFil intermediate filament, TM transmembrane, GPCR G protein–coupled receptor, ECM extracellular matrix).

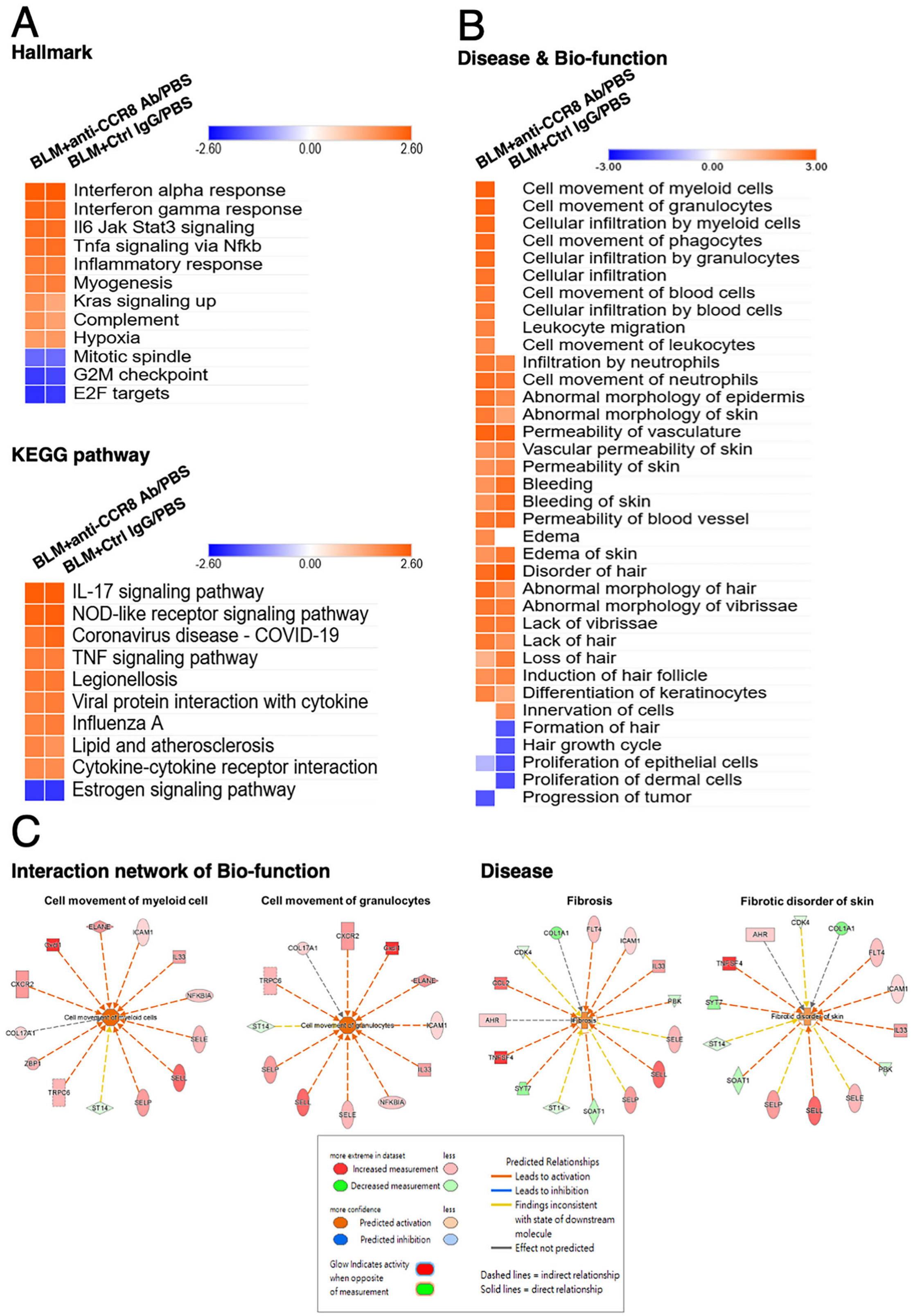

Fig. 9 | Gene set enrichment analysis and ingenuity pathway analysis of bleomycin-induced systemic sclerosis mouse model. A Heatmap showing significant Hallmark pathways and the top 10 enriched Kyoto Encyclopedia of Genes and Genomes (KEGG) pathways from Gene Set Enrichment Analysis (GSEA). **B** Ingenuity Pathway Analysis (IPA)-predicted Disease and Bio-functions with |z score| ≥ 2 in at least one group were included for visualization. Notably, inflammation- and cell movement–related functions are prominently activated in the bleomycin (BLM) + anti-C-C motif chemokine receptor 8 (CCR8) Ab group. **C** Interaction networks of the top two activated biological functions in the BLM + anti-CCR8 antibody (Ab) vs. phosphate buffer saline (PBS) group, including “Cell movement of myeloid cells” and “Cell movement of granulocytes.” The disease categories “Fibrosis” and “Fibrotic disorder of skin” also show higher enrichment in the BLM + anti-CCR8 Ab group compared to the BLM + Ctrl IgG group, suggesting a stronger fibrotic response modulated by anti-CCR8 Ab treatment.

Together, these results support a mechanistic role for CCR8-targeting autoantibodies in modulating disease activity.

Importantly, several of the GPCRs targeted by autoantibodies we identified are biologically plausible in the context of SSc. For example, FPR1 mediates neutrophil activation in response to mitochondrial peptides such as fMet, which are elevated in SSc patients and promote inflammation[45]. MC1R, expressed on skin fibroblasts and vascular endothelium, mediates anti-inflammatory responses and is currently under clinical investigation as a therapeutic target for SSc[46]. Nevertheless, it is important to recognize that the pathogenic potential of an autoantibody is not necessarily reflected by its serum concentration. Some GPCR-targeting autoantibodies exert biological effects at low titers, and both excess and deficiency of such antibodies have been implicated in human disorders[47–49]. As our screening focused on antibodies elevated in SSc relative to HCs, we may have overlooked functionally relevant antibodies present at low or regulated levels. Additionally, the use of recombinant proteins in a cell-free expression system may have limited the detection of conformational or membrane-dependent epitopes. These considerations highlight the need for complementary methods—such as cell-based or other conformation-preserving assays[50,51]—to comprehensively capture the functional autoantibody landscape in SSc.

Several limitations must be acknowledged. First, given the absence of standardized criteria for defining treatment response in SSc in the context of B-cell–depleting therapy, our threshold for high response was selected to optimize statistical power while maintaining clinical interpretability. Nonetheless, this classification remains exploratory, and future studies with larger sample sizes will be essential for refining response definitions and improving stratification strategies in RTX-treated SSc. Second, although we performed multiple comparison adjustment using the Benjamini–Hochberg method, no candidate fulfilled all criteria—elevation in SSc, enrichment in HRs, and reduction post-RTX. Therefore, our primary analyses used an uncorrected significance threshold ($P < 0.05$), increasing the risk of false positives. While our analyses were based on a well-characterized, placebo-controlled clinical trial, the lack of external validation limits the generalizability of the identified autoantibody signatures. Future studies incorporating larger, independent datasets and orthogonal validation methods are required to substantiate the clinical utility of the identified autoantibody signatures. Third, although anti-CCR8 autoantibodies were functionally validated, the majority of the 88 candidate autoantibodies remain uncharacterized to determine antigen specificity, causality, and downstream biological effects. It is therefore possible that some represent epiphenomena of immune activation rather than bona fide contributors to disease pathogenesis. These findings should thus be interpreted as immunological correlates rather than definitive indicators of causality. Fourth, although our study met its predefined primary endpoint based on mRSS, this clinical parameter has inherent limitations. Skin fibrosis in SSc may exhibit spontaneous improvement over time, making it difficult to disentangle treatment effects from the natural disease course. Moreover, mRSS reflects only cutaneous involvement and may not capture the full systemic burden of disease. In particular, ILD—the leading cause of SSc-related mortality—was not uniformly present among study participants and was not the primary endpoint in this trial. While our dataset lacked the statistical power to formally evaluate lung-specific endpoints, our analyses identified negative correlations between serum levels of selected anti-GPCR autoantibodies (e.g., anti-P2RY8 and anti-FPR1) and forced vital capacity of the lung. These findings raise the possibility that some autoantibodies may be linked to pulmonary involvement and merit further investigation in ILD-enriched cohorts.

In conclusion, this study integrates comprehensive autoantibody profiling with functional analyses in vitro and in vivo to explore the immunopathology of SSc. Our approach, which we term "autoantigenomics"[39], highlights the utility of longitudinal autoantibody dynamics as biomarkers of treatment response and underscores the potential biological relevance of novel antibody specificities such as anti-CCR8. Future studies should aim to validate these findings in larger, multi-organ cohorts, apply rigorous correction for multiple comparisons, and explore structural and functional properties of additional candidates to fully elucidate their roles in disease pathogenesis and therapy.

Methods

Study design

The study design for the DESIRES trial has been previously reported (NCT04274257)[30]. The full protocol of the trial is available at https://clinicaltrials.gov/study/NCT04274257. Briefly, the DESIRES trial was a randomized, double-blind, placebo-controlled trial of 24 weeks. The primary endpoint of the double-blind phase was the absolute change in mRSS 24 weeks after 13 intervention initiation compared to the baseline. In total, 56 patients were randomized to receive either intravenous rituximab (375 mg/m^2) or matching placebo once per week for 4 weeks, based on the allocation factors of 4 disease duration (≤6 years or >6 years), mRSS (≥20 or <20), and concomitant ILD (present or absent) by the minimization method. Of these, 49 patients completed the double-blind phase. Serum samples were collected and served for PWAbS at the beginning and the end of the double-blind phase (Fig. 1A). After excluding 4 cases due to their serum unsuitable for PWAbS, data of 45 patients were included in our analysis. Age and sex matched HCs were selected from a cohort of healthcare providers on annual checkups without any medical history (Fig. 1B), using 'matchIt' R package[52]. This study was approved by the ethics committee of the University of Tokyo Graduate School of Medicine and conducted in accordance with the Declaration of Helsinki. Written informed consent was obtained from all patients.

Assessments

Clinical and laboratory assessments were performed at baseline and at 24 weeks after the first infusion of RTX. Skin sclerosis was assessed by mRSS[53]. Presence and severity of interstitial lung disease (ILD) was judged upon occupied area of interstitial shadows (reticular changes, honeycombing, and ground-glass opacities) by high-resolution CT. Lung function was evaluated by pulmonary function tests. Serum levels of Krebs von den Lungen-6 (KL-6), surfactant protein-A (SP-A), and surfactant protein-D (SP-D) were measured as established markers of ILD in patients with SSc. Laboratory examinations included serum levels of immunoglobulin G (IgG), immunoglobulin M (IgM), immunoglobulin A (IgA), brain natriuretic peptide (BNP). Serum levels of anti-topoisomerase I antibody (ATA), anti-centromere antibody (ACA), anti-RNA polymerase III antibody (ARA), and anti-ribonucleoprotein antibody (RNP) were measured by enzyme-linked immunosorbent assays (ELISA). Quality of life was assessed using the medical outcomes study 36-item short-form general health survey (SF-36) and health assessment questionnaire disability index (HAQ-DI). High responders (HRs) were defined as patients who achieved a ≥7-point decrease in mRSS over 24 weeks, while those with a ≤6-point change were classified as low responders (LRs). This cutoff was selected to (1) exceed the minimal clinically important difference reported in previous studies[54], (2) reflect the shorter time frame compared to typical 12-month endpoints, and (3) ensure a balanced distribution of patients to maximize statistical power within our modest sample size. Based on this definition, 16 patients were classified as HRs and 13 as LRs (Fig. 2B).

Autoantibody measurement

WPAs were arranged as follows[33]. First, proteins were synthesized in vitro utilizing a wheat germ cell-free system from 13,455 clones of the HuPEX[31]. POLR3A and TRIM21 existed in two forms: full-length and truncated. 'TRIM21(1-400)' indicates a truncated version of TRIM21, covering amino acids 1 to 400, and lacks the protein's immunoglobulin-binding domains. This truncated version was included in the database to avoid the difficulties in differentiating autoantibody signals from background noise due to the binding nature of full-length TRIM21. 'POLR3A_D' represents a truncated form of POLR3A (RNA polymerase III), which improves anti-RNA polymerase III antibody detection. All other proteins were full-length. Second, synthesized proteins were plotted onto glass plates (#S339009, Matsunami Glass, Osaka, Japan) in an array format by the affinity between the GST-tag added to the N-terminus of each protein and glutathione modified on the plates. The WPAs were treated with human serum diluted by 3:1000 in the reaction buffer containing 1x Synthetic block (Invitrogen), PBS, and 0.1% Tween 20. Next, the WPAs were washed, and goat anti-Human IgG (H + L) Alexa Flour 647 conjugate (#A-21445, Thermo Fisher Scientific, San Jose, CA, USA) diluted 1000-fold was added to the WPAs and reacted for 1 h at room temperature. Finally, the WPAs were washed, air-dried, and fluorescent images were acquired using a fluorescence imager (Typhoon FLA 9500, Cytiva, Marlborough, MA, USA). Fluorescence images were analyzed to quantify serum levels of autoantibodies targeting each antigen, following the formula shown below:

$$Autoantibody\ level\,[AU] = \frac{F_{autoantigen} - F_{negative\ control}}{F_{positive\ control} - F_{negative\ control}} \times 100$$

AU: arbitrary unit

$F_{autoantigen}$: fluorescent intensity of autoantigen spot

$F_{negative\ control}$: fluorescent intensity of the negative control spot

$F_{positive\ control}$: fluorescent intensity of the positive control spot

Machine learning

We applied supervised machine learning techniques using the Python code with the 'scikit-learn' library to analyze the autoantibody measurement data. With the random forest model, decision trees were built and trained in parallel on subsets of sampled instances and features. Meanwhile, with the XGBoost model, decision trees were built sequentially to improve each other. The final prediction of the random forest was based on the majority of its decision trees, while that of XGBoost was derived from their weighted average. The performance of the classifiers was evaluated by 5-fold cross-validation, using the area under the operator-receiver operating characteristic curve (AUC), accuracy, precision, recall, and F1-score, with the higher the scores indicating the better classification performance. The accuracy is the ratio of the correct positive and negative predictions, the precision is the ratio of the correct positive predictions, the recall (or sensitivity) is the ratio of the correct positive predictions among all true positive instances, and the F1-score is the harmonic mean of precision and sensitivity.

WGCNA analysis

The analysis included 135 specimens from SSc patients at week 0 ($n = 45$) and week 24 ($n = 45$), as well as HCs ($n = 45$). The weighted correlation network was constructed using the 'WGCNA' R package[40]. We calculated each gene pair's Pearson correlation coefficient, measured how similar their expressions were, and created a correlation matrix. Scale-free topology requirements were used to compute the 'soft' threshold power to build biologically meaningful scale-free networks. Based on the adjacency matrix, dynamic tree cuts and at least 100 genes per module were utilized to generate a topological overlap matrix for co-expression modules. In addition, we assessed gene significance, module membership, and correlated modules with clinical characteristics and mapped signature genes.

Generation of HEK293 cells overexpressing CCR8

Human CCR8 was stably overexpressed in HEK293 cells using a lentiviral transduction system. Lentiviral particles were generated carrying the *pLV[Exp]-Puro-CMV > hCCR8[NM_005201.4]* construct (Supplementary Fig. 4A and Supplementary Data 6; VectorBuilder, Yokohama, Japan). HEK293 cells (ATCC CRL-1573, Lot No. 70047548) were purchased from the American Type Culture Collection (ATCC, Manassas, VA, USA). This cell line is not listed in the International Cell Line Authentication Committee database of misidentified or cross-contaminated cell lines. Cell line identity was verified by short tandem repeat profiling, confirming a match to the reference HEK293 profile. Cells tested negative for mycoplasma contamination using a PCR-based assay (last tested on May 17, 2025). Cells were used within 10 passages after thawing for all experiments. HEK293 cells were cultured in Dulbecco's Modified Eagle Medium (DMEM) with 4.5 g/L glucose and 4 mM L-glutamine (#G7513, Sigma Aldrich, St. Luis, MO, USA) supplemented with 10% fetal bovine serum under standard conditions (37 °C, 5% CO_2), and subcultured every 2–3 days at a 1:3–1:4 split ratio. Cells were transduced with the CCR8-expressing lentivirus and selected using puromycin (1.5 µg/mL) for 3–5 days. Following antibiotic selection, stable cell pools were maintained in 0.75 µg/mL puromycin for downstream validation.

RT-qPCR

Total RNA was extracted from transfected and wild-type HEK293 cells, followed by cDNA synthesis. Quantitative real-time PCR was conducted using primers specific for human *CCR8* and *GAPDH* (housekeeping gene). Relative expression levels were calculated using the ΔΔCt method. The sequence of the primers used is shown in Supplementary Table 2.

Immunocytochemistry

Cells were also seeded on glass coverslips covered by poly-L-lysine (#28356-84, Nakalai Tesque, Osaka, Japan, 1:100 dilution), fixed with −20°C acetone (#013-00356, FUJIFILM Wako Pure Chemical Corporation, Osaka, Japan), and permeabilized with 0.1% Triton X-100 (#35501-12, Nakalai Tesque, Osaka, Japan, 1:1000 dilution). After blocking with 5% goat serum in PBS, cells were incubated with APC-conjugated primary anti-CCR8 antibody (#566897, BD Biosciences, Franklin Lakes, NJ, USA, 1:100 dilution) overnight at 4 °C. Nuclei were counterstained with VECTASHIELD Mounting Medium with DAPI (#H-1200, Vector Laboratories, Newark, CA, USA) and observed by BZ-X1000 (Keyence, Osaka, Japan).

Isolation of IgG fractions from human sera

IgG fractions were purified from human serum samples using a combination of protein G affinity chromatography, dialysis, and ultrafiltration. Briefly, serum was diluted with binding buffer, applied to a Protein G column (#17112801, Cytiva, Marlborough, MA, USA) and then eluted according to the manufacturer's instructions. The eluate was then subjected to buffer exchange and removal of low molecular weight components using 10 K molecular weight cut-off dialysis cassettes (#66810, Thermo Fisher Scientific, Waltham, MA, USA). Subsequently, the IgG fraction was concentrated using 10 K molecular weight cut-off centrifugal devices (#88528, Thermo Fisher Scientific). Purified IgG was quantified by absorbance at 280 nm using NanoDrop One (Thermo Fisher Scientific), aliquoted, and stored at −80 °C until use in downstream assays.

Flow cytometry

Live HEK293 cells were collected and washed by PBS. After blocking by 1% FBS and Fc receptor blocking solution (#422301, BioLegend, San Diego, CA, USA, 1:100 dilution) with or without anti-CCR8 antibody (#566897, BD Biosciences, 1:100 dilution), the cells were stained with IgG fraction extracted from anti-CCR8 seropositive SSc sera ($n = 4$) or from anti-CCR8 seronegative HC at 1 µg/mL ($n = 4$), followed by staining by PE-conjugated secondary anti-human IgG Fc antibody (#410707, BD Biosciences, 1:100 dilution) and 7-AAD viability staining solution (#420403, BioLegend, San Diego, CA, USA, 1:100 dilution).

Flow cytometric analysis was conducted using a CytoFLEX S (Beckman Coulter, Brea, CA, USA) and Kaluza (Beckman Coulter). Gating strategy is shown in Supplementary Fig. 6.

ERK phosphorylation assay

Transfected HEK293 cells were seeded in 24-well plates and cultured for 24 hours. Following serum starvation for 4 hours, the cells were stimulated for 3 minutes under the following conditions: no treatment ($n = 4$), CCL1 alone (100 ng/mL; $n = 4$), CCL1 with healthy control IgG (1 μg/mL; $n = 4$), or CCL1 with IgG purified from anti-CCR8 seropositive SSc patient serum (1 μg/mL; $n = 4$). Levels of total ERK and phosphorylated ERK were measured using an ELISA kit (#176640, Abcam, Cambridge, UK) according to the manufacturer's instructions.

Regulatory T cell (Treg) isolation from whole blood

Tregs were isolated from human peripheral blood using the MACSxpress Whole Blood Treg Isolation Kit (#130-109-557, Miltenyi Biotec, Bergisch Gladbach, North Rhine-Westphalia, Germany), following the manufacturer's instructions with minor modifications. Briefly, 6 mL of EDTA-anticoagulated whole blood was mixed with 500 μL/mL MACS Separation Buffer (#130-091-221, Miltenyi Biotec) and 50 μL/mL Treg Isolation Cocktail. After incubation on a tube rotator at 12 rpm for 10 minutes, samples were placed in a MACSxpress Separator (Miltenyi Biotec) for magnetic depletion. The $CD4^+$ fraction was collected and further purified using LS columns (#130-042-401, Miltenyi Biotec), yielding $CD4^+CD25^+$ Treg cells. Cells were pelleted by centrifugation (400 × *g*, 5 min, RT) and resuspended in ImmunoCult-XF T Cell Expansion Medium (# 10981, STEMCELL Technologies, Vancouver, BC, Canada) at 2×10^6 cells/mL.

Treg culture and expansion

Fresh complete T cell expansion medium was prepared by supplementing ImmunoCult-XF medium with recombinant IL-2 (#202-IL-010, 100 U/mL; R&D Systems, Minneapolis, MN, USA), rapamycin (#73364, 100 nM; STEMCELL Technologies), and ImmunoCult Human CD3/CD28 T Cell Activator (#10971, 25 μL/mL; STEMCELL Technologies). Tregs were cultured at a density of 1×10^6 cells/mL and maintained at 37 °C in 5% CO_2. On days 3 and 6, cells were harvested, counted, and re-seeded in fresh complete medium at $1–2.5 \times 10^5$ cells/mL. Cytokine concentrations were maintained throughout culture. After 9 days, Tregs were re-stimulated for 24 hours with CD3/CD28 (12.5 μL/mL) and IL-2 (25 ng/mL) prior to the migration assay.

Transwell migration assay

Following expansion, Tregs were washed and resuspended in PBS containing 1% BSA. Migration assays were conducted using 6.5 mm Transwell® inserts (#3421, 5.0 μm pore, Corning, Corning, NY, USA). The lower chambers were filled with 600 μL of PBS with 1% fetal bovine serum containing CCR8 ligands: CCL1 (#272-I-010, R&D Systems, 100 ng/mL; $n = 6$), CCL1 and healthy control IgG (1 μg/mL; $n = 6$), or CCL1 and anti-CCR8 IgG purified from SSc patient serum (1 μg/mL; $n = 6$). Tregs (5×10^5 cells/well) were seeded in the upper chambers (100 μL/well). All wells received vehicle-matched controls. Plates were incubated at 37 °C and 5% CO_2 for 2 hours. Migrated cells in the lower chamber were collected and stained with FITC-anti-human CD4 (#555346, BD Biosciences) and APC-anti-human CD25 (#555434, BD Biosciences) in PBS, incubated at 4 °C for 30 minutes, washed, and fixed with BD Cytofix Fixation Buffer (#554655, BD Biosciences). Stained cells were analyzed using a flow cytometer to determine the number of migrated CD4, CD25 double-positive cells. Gating strategy is illustrated in Supplementary Fig. 7.

Bleomycin (BLM)-induced SSc mouse model

Pathogen-free, wild-type female C57BL/6NcrSlc mice (MGI ID: MGI:5295404; 6 weeks old) were purchased from Japan SLC, Inc. (Hamamatsu, Shizuoka, Japan), as SSc predominantly affects females in humans and the use of female mice provides a more representative model of disease biology. All mice were housed in an air-filtered clean room under controlled conditions (temperature: 21 ± 1 °C; relative humidity: 60 ± 10%) with a 12-h light/dark cycle. Experimental and control animals were housed under identical conditions to minimize environmental variation. Bleomycin (BLM; Nippon Kayaku, Tokyo, Japan) was dissolved in PBS at a concentration of 1 mg/mL. To induce skin sclerosis, 200 μg of BLM was administered subcutaneously into the shaved dorsal skin of mice once daily for 14 consecutive days using a 30-gauge needle. Control mice received an equal volume of PBS following the same injection protocol. Terminate parameters were established in accordance with the guidelines of the Animal Experiment Committee of the University of Tokyo (Approval number: A2024M092-01). Mice were euthanized if they exhibited feeding or drinking difficulties, signs of distress (such as self-injury, abnormal posture, respiratory distress, or vocalization), persistent external abnormalities without recovery (including diarrhea, bleeding, or genital soiling), or rapid body weight loss exceeding 20% over several days. All experiments strictly adhered to these criteria.

Anti-CCR8 antibody treatment and experimental design

To investigate the potential role of anti-CCR8 Ab in the pathogenesis of systemic sclerosis, a single intraperitoneal injection (200 μL) was administered on day 8 after the initiation of BLM treatment. Six-week-old C57BL/6NcrSlc female mice received either anti-mouse CCR8 monoclonal Ab (#12025; 100 μg/mouse; 0.5 mg/mL; BioLegend) or an isotype-matched rat IgG2b κ control IgG (#400633, 100 μg/mouse; 0.5 mg/mL; BioLegend). The dosage and timing were determined based on preliminary experiments. Experimental groups included six mice in the PBS control group, and five mice in each in the BLM + anti-CCR8 Ab group and the BLM + control IgG group. All procedures involving animals were performed in accordance with the guidelines for animal experimentation of the University of Tokyo and were approved by the Animal Experiment Committee of its Graduate School of Medicine (approval number: A2024M092-01).

Histological analysis

Mice were euthanized by cervical dislocation following anesthesia with isoflurane inhalation (FUJIFILM Wako Pure Chemical Corporation), in accordance with the institutional animal care guidelines. Dorsal skin tissues were collected and bisected. One half of each tissue sample was immediately fixed in MildformR 10 N (#133-10311, FUJIFILM Wako Pure Chemical Corporation) for histopathological analysis, while the other half was preserved in RNAlater RNA Stabilization Solution (#AM-7021, Thermo Fisher Scientific) and stored at −80 °C for subsequent RNA extraction and transcriptomic profiling. The fixed skin specimens were embedded in paraffin, sectioned, deparaffinized, and rehydrated. Hematoxylin and eosin (H&E) staining, Masson's trichrome staining, and immunohistochemistry utilizing anti-Foxp3 antibody (#12653, Cell signaling technology, Danvers, MA, USA) were performed following standard histological protocols. Stained sections were imaged using a bright-field microscope for histological evaluation.

RNA extraction and next-generation sequencing

Total RNA was extracted from all nine RNAlater-preserved skin tissue samples using the RNeasy Mini Kit (#74106, Qiagen, Hilden, Germany) according to the manufacturer's instructions. Briefly, tissues were homogenized in Buffer RLT supplemented with β-mercaptoethanol (#444203, Sigma Aldrich) using a TissueLyser II (Qiagen) in microcentrifuge tubes. To eliminate genomic DNA contamination, an on-column DNase digestion step was performed as described in the manufacturer's protocol. The resulting purified RNA was quantified and assessed using a NanoDrop One spectrophotometer (Thermo Fisher Scientific), and samples with the highest RNA quality from three mice per group were selected for next-generation sequencing. Library construction and sequencing were performed by NovaSeq X Plus (Illumina, San Diego, CA, USA). Read alignment was performed using the STAR aligner[55] against the mouse reference genome (GRCm38, version M18).

Differential gene expression and visualization

Differential expression analysis was conducted using DESeq2 (v1.46.0)[54] to identify differentially expressed genes (DEGs) across three experimental comparisons: BLM + anti-CCR8 Ab vs. PBS, BLM + control IgG vs. PBS, and BLM + anti-CCR8 Ab vs. BLM + control IgG. Genes with an adjusted p-value (Benjamini–Hochberg corrected) <0.05, an absolute $\log_2$ fold change > 1 (calculated based on the mean normalized counts between conditions) were defined as DEGs. In addition, genes with low expression (TPM < 0.3) in both conditions were excluded from further analysis.

To visualize gene expression patterns, transcript-level TPM values were derived from RNA-seq data. These values were $\log_2$-transformed [$\log_2$ (TPM + 1)] to stabilize variance across genes. The union set of DEGs from all comparisons was selected, and the expression values for these genes were scaled by row (gene-wise Z-score). A heatmap was then generated using the '*pheatmap*' package (v1.0.12) in R (v4.3.2).

To further illustrate DEG patterns, volcano plots were generated for each comparison using the '*EnhancedVolcano*' package (v1.24.0). Genes were plotted according to their $\log_2$ fold change and adjusted p-values. Significant genes were color-coded to indicate upregulation or downregulation.

Gene ontology (GO) enrichment analysis of DEGs

To explore the biological functions associated with DEGs, Gene Ontology (GO) enrichment analyses were performed using the '*clusterProfiler*' package (v4.14.6) in R. DEGs ($|\log_2$ fold change$| > 1$, adjusted p-value < 0.05, TPM > 0.3 in either condition) were included from further analysis[56]. GO enrichment was evaluated across the categories of Biological Process (BP), Molecular Function (MF), and Cellular Component (CC). GO terms with a Benjamini–Hochberg corrected p-value < 0.05 were considered significantly enriched. Representative bubble plots were generated to display the top 10 enriched pathways for each category.

Gene set enrichment analysis using hallmark and KEGG pathways

Gene Set Enrichment Analysis (GSEA) was performed to evaluate the enrichment of biologically meaningful pathways based on gene expression changes using the '*clusterProfiler*' package in R (v4.14.6)[57]. Only genes with TPM > 0.3 in either condition were included in the analysis. All retained genes were ranked by their log2 fold change values. This complete ranked gene list was used as input for enrichment testing. For Hallmark GSEA, gene sets were obtained from the Molecular Signatures Database (MSigDB, category 'H') for *Mus musculus*. Statistical significance was defined as an adjusted p-value < 0.05. Normalized enrichment scores (NES) were extracted, and pathways with p < 0.05 were visualized heatmap. Color gradients represented the direction and magnitude of enrichment. For KEGG-based GSEA, gene symbols were first mapped to Entrez Gene IDs using the org.Mm.eg.db annotation database. The analysis was performed using the ranked Entrez ID-based gene list as input. Similar visualization procedures were applied.

Ingenuity pathway analysis (IPA)

Gene expression profiles, including $\log_2$ fold change values and adjusted p-value of DEGs from mouse skin tissue samples, were uploaded to the Ingenuity Pathway Analysis (IPA, Qiagen) software platform[58], as previously described[59,60]. Core analysis was performed to predict significantly enriched diseases and bio-functions, canonical pathways, upstream regulators, and related molecular interaction networks. The activation state of predicted pathways and regulators was inferred using the IPA z-score algorithm, which evaluates consistency between the observed gene expression patterns and curated directional interactions in the Ingenuity Knowledge Base. Pathways with an absolute z-score ≥2 were considered significantly activated or inhibited.

Statististics and reproducibility

Fisher's exact test was performed to compare categorical variables. For experiments involving two groups, the Mann–Whitney U test or Wilcoxon signed-rank test was used as appropriate. Multiple comparison adjustment was conducted by Benjamini & Hochberg method. For experiments involving more than two groups, Welch's ANOVA followed by Dunnett's T3 multiple comparison adjustment was applied. Spearman's correlation test was used for correlation analysis. P values < 0.05 were considered statistically significant. Data analyses were conducted using R (v4.2.1) or Prism (v.10.1.1, GraphPad Software, MA, USA). No statistical method was used to predetermine sample size. No data were excluded from the analyses. Animals were allocated to the BLM-treated or control groups according to the experimental design rather than by randomization. All mice were age- and sex-matched and housed under identical specific pathogen-free conditions to minimize variability and control for covariates. Investigators were not blinded to group allocation during the BLM-induced mouse experiments because BLM treatment produces visible skin changes that make the treatment groups readily distinguishable. Blinding was therefore not feasible for these experiments.

Data visualization

Box plots, scatter plots, hierarchical clustering, and correlation matrix were visualized by using R (v4.2.1). Box plots were defined as follows: the middle line corresponds to the median; the lower and upper hinges correspond to the first and third quartiles; the upper whisker extends from the hinge to the largest value no further than 1.5 times the interquartile range (IQR) from the hinge; and the lower whisker extends from the hinge to the smallest value at most 1.5 times the IQR of the hinge.

Reporting summary

Further information on research design is available in the Nature Portfolio Reporting Summary linked to this article.

Data availability

The RNA sequencing data have been deposited in the DDBJ Sequence Read Archive under the accession number DRA021712. The raw numbers for charts and graphs are available in the Source Data file whenever possible. The clinical autoantibody dataset cannot be made publicly available due to restrictions specified in the informed consent and approved by the institutional ethics committee. Access to these data is available under controlled conditions for academic research purposes. Requests should be directed to the corresponding author, and will require confirmation of an appropriate data use agreement and ethics approval. All other data supporting the findings of this study are included in the Supplementary Information and Supplementary Data. Source data are provided with this paper.

Code availability

All the scripts are available at https://github.com/mkazukikom/RTXML.

References

1. Allanore, Y. et al. Systemic sclerosis. *Nat. Rev. Dis. Prim.* **1**, 1–21 (2015).
2. Rubio-Rivas, M., Royo, C., Simeón, C. P., Corbella, X. & Fonollosa, V. Mortality and survival in systemic sclerosis: Systematic review and meta-analysis. *Semin. Arthritis Rheum.* **44**, 208–219 (2014).

3. Matsuda, K. M. et al. Skin thickness score as a surrogate marker of organ involvements in systemic sclerosis: a retrospective observational study. *Arthritis Res. Ther.* **21**, 129 (2019).
4. Hasegawa, M. et al. B-lymphocyte depletion reduces skin fibrosis and autoimmunity in the tight-skin mouse model for systemic sclerosis. *Am. J. Pathol.* **169**, 954–966 (2006).
5. Numajiri, H. et al. B Cell depletion inhibits fibrosis via suppression of profibrotic macrophage differentiation in a mouse model of systemic sclerosis. *Arthritis Rheumatol.* **73**, 2086–2095 (2021).
6. Fukasawa, T. et al. Single-cell-level protein analysis revealing the roles of autoantigen-reactive B lymphocytes in autoimmune disease and the murine model. https://doi.org/10.7554/eLife.
7. Frantz, C., Auffray, C., Avouac, J. & Allanore, Y. Regulatory T cells in systemic sclerosis. *Front. Immunol.* **9**, 2356 (2018).
8. Kobayashi, S., Nagafuchi, Y., Shoda, H. & Fujio, K. The pathophysiological roles of regulatory T cells in the early phase of systemic sclerosis. *Front. Immunol.* **13**, 900638 (2022).
9. Sekiguchi, A. et al. Inhibition of skin fibrosis via regulation of Th17/Treg imbalance in systemic sclerosis. *Sci. Rep.* **15**, 1423 (2025).
10. Asano, Y. The pathogenesis of systemic sclerosis: An understanding based on a common pathologic cascade across multiple organs and additional organ-specific pathologies. *J. Clin. Med.* **9**, 1–27 (2020).
11. Daoussis, D. et al. A multicenter, open-label, comparative study of B-cell depletion therapy with Rituximab for systemic sclerosis-associated interstitial lung disease. *Semin. Arthritis Rheum.* **46**, 625–631 (2017).
12. Sircar, G., Goswami, R. P., Sircar, D., Ghosh, A. & Ghosh, P. Intravenous cyclophosphamide vs rituximab for the treatment of early diffuse scleroderma lung disease: Open label, randomized, controlled trial. *Rheumatol. (U. Kingd.)* **57**, 2106–2113 (2018).
13. Ebata, S. et al. Rituximab therapy is more effective than cyclophosphamide therapy for Japanese patients with anti-topoisomerase I-positive systemic sclerosis-associated interstitial lung disease. *J. Dermatol.* **46**, 1006–1013 (2019).
14. Einhaus, J. et al. Inhibition of effector B cells by ibrutinib in systemic sclerosis. *Arthritis Res. Ther.* **22**, 1–8 (2020).
15. Matsuda, K. M. et al. An open-label randomized parallel-group phase I study of the oral Bruton tyrosine kinase inhibitor tirabrutinib in systemic sclerosis. *Br. J. Dermatol.* **in press**, (2025).
16. Ando, T. & Oda, H. Bruton tyrosine kinase inhibition in systemic sclerosis: a promising new B-cell therapy. *Br. J. Dermatol.* ljaf202 https://doi.org/10.1093/bjd/ljaf202 (2025).
17. Bergmann, C. et al. Treatment of a patient with severe systemic sclerosis (SSc) using CD19-targeted CAR T cells. *Ann. Rheum. Dis.* **82**, 1117–1120 (2023).
18. Merkt, W. et al. Third-generation CD19.CAR-T cell-containing combination therapy in Scl70+ systemic sclerosis. *Ann. Rheum. Dis.* **83**, 543 LP–543546 (2024).
19. Fabian, M. et al. CD19 CAR T-cell therapy in autoimmune disease — a case series with follow-up. *N. Engl. J. Med.* **390**, 687–700 (2024).
20. Sakkas, L. I., Katsiari, C. G., Daoussis, D. & Bogdanos, D. P. The role of B cells in the pathogenesis of systemic sclerosis: an update. *Rheumatology* **62**, 1780–1786 (2023).
21. Malasheuskaya, A. et al. Regulatory T-cell immunotherapy as treatment of systemic sclerosis. *J. Allergy Clin. Immunol.* **155**, AB27 (2025).
22. Ebata, S. et al. Safety and efficacy of rituximab in systemic sclerosis (DESIRES): open-label extension of a double-blind, investigators-initiated, randomised, placebo-controlled trial. *Lancet Rheumatol.* **4**, e546–e555 (2022).
23. Kuzumi, A. et al. Long-term outcomes after rituximab treatment for patients with systemic sclerosis: follow-up of the DESIRES Trial With a Focus on Serum Immunoglobulin Levels. *JAMA Dermatol.* **159**, 374–383 (2023).
24. Ebata, S. et al. Predictors of rituximab effect on modified Rodnan skin score in systemic sclerosis: a machine-learning analysis of the DesiReS trial. *Rheumatology* **61**, 4364–4373 (2022).
25. Kuzumi, A. et al. Predictors of rituximab efficacy in systemic sclerosis-associated interstitial lung disease: machine-learning analysis of the DESIRES trial. *Rheumatology* keae716 https://doi.org/10.1093/rheumatology/keae716 (2024).
26. Stasi, R. et al. Analysis of regulatory T-cell changes in patients with idiopathic thrombocytopenic purpura receiving B cell–depleting therapy with rituximab. *Blood* **112**, 1147–1150 (2008).
27. Bhatia, D. et al. Rituximab modulates T- and B-lymphocyte subsets and urinary CD80 excretion in patients with steroid-dependent nephrotic syndrome. *Pediatr. Res.* **84**, 520–526 (2018).
28. Okano, Y. Antinuclear antibody in systemic sclerosis (scleroderma). *Rheum. Dis. Clin. North Am.* **22**, 709–735 (1996).
29. Nihtyanova, S. I. & Denton, C. P. Autoantibodies as predictive tools in systemic sclerosis. *Nat. Rev. Rheumatol.* **6**, 112–116 (2010).
30. Ebata, S. et al. Safety and efficacy of rituximab in systemic sclerosis (DESIRES): a double-blind, investigator-initiated, randomised, placebo-controlled trial. *Lancet Rheumatol.* **3**, e489–e497 (2021).
31. Goshima, N. et al. Human protein factory for converting the transcriptome into an in vitro-expressed proteome. *Nat. Methods* **5**, 1011–1017 (2008).
32. Fukuda, E. et al. Identification and characterization of the antigen recognized by the germ cell mAb TRA98 using a human comprehensive wet protein array. *Genes Cells* **26**, 180–189 (2021).
33. Matsuda, K. M. et al. Autoantibody landscape revealed by wet protein array: sum of autoantibody levels reflects disease status. *Front. Immunol.* **13**, 1–14 (2022).
34. Kuzumi, A. et al. Comprehensive autoantibody profiling in systemic autoimmunity by a highly-sensitive multiplex protein array. *Front. Immunol.* **14**, 10.3389/fimmu.2023.1255540 (2023).
35. Matsuda, K. M., Kotani, H., Yamaguchi, K., Okumura, T. & Fukuda, E. Significance of anti-transcobalamin receptor antibodies in cutaneous arteritis revealed by proteome-wide autoantibody screening. *J. Autoimmun.* **135**, 102995 (2023).
36. Matsuda, K. M. et al. Autoantibodies to nuclear valosin-containing protein-like protein: systemic sclerosis-specific antibodies revealed by in vitro human proteome. *Rheumatol. (Oxf.)* https://doi.org/10.1093/rheumatology/keae063 (2024).
37. Matsuda, K. M. et al. Artificial intelligence and omics-based autoantibody profiling in dementia. *Front Immunol.* **16**, 1537659 (2025).
38. Kotani, H. et al. Diversity and Epitope Spreading of Anti–RNA Polymerase III Antibodies in Systemic Sclerosis: A Potential Biomarker for Skin and Lung Involvement. *Arthritis Rheumatol.* **77**, 67–79 (2024).
39. Matsuda, K. M. et al. Proteome-wide autoantibody screening and holistic autoantigenomic analysis unveil COVID-19 signature of autoantibody landscape. *medRxiv* 2024.06.07.24308592 (2024).
40. Langfelder, P. & Horvath, S. WGCNA: An R package for weighted correlation network analysis. *BMC Bioinformatics* **9**, 559 (2008).
41. Spinetti, G. et al. The chemokine receptor CCR8 mediates rescue from dexamethasone-induced apoptosis via an ERK-dependent pathway. *J. Leukoc. Biol.* **73**, 201–207 (2003).
42. Barsheshet, Y. et al. CCR8+FOXp3+ Treg cells as master drivers of immune regulation. *Proc. Natl Acad. Sci.* **114**, 6086–6091 (2017).
43. Fagerberg, L. et al. Analysis of the human tissue-specific expression by genome-wide integration of transcriptomics and antibody-based proteomics. *Mol. Cell. Proteom.* **13**, 397–406 (2014).
44. The Tabula Sapiens Consortium. The Tabula Sapiens: A multiple-organ, single-cell transcriptomic atlas of humans. *Sci. (80-.)* **376**, eabl4896 (2022).
45. Kuley, R. et al. N-Formyl Methionine Peptide-Mediated Neutrophil Activation in Systemic Sclerosis. *Front Immunol.* **12**, 785275 (2022).

46. Kondo, M. et al. Dersimelagon, a novel oral melanocortin 1 receptor agonist, demonstrates disease-modifying effects in preclinical models of systemic sclerosis. *Arthritis Res. Ther.* **24**, 210 (2022).
47. Klapa, S. et al. Low Concentrations of C5a complement receptor antibodies are linked to disease activity and relapse in anti-neutrophil cytoplasmic autoantibody–associated vasculitis. *Arthritis Rheumatol.* **75**, 760–767 (2023).
48. Ernst, D. et al. Lowered anti-beta1 adrenergic receptor antibody concentrations may have prognostic significance in acute coronary syndrome. *Sci. Rep.* **9**, 14552 (2019).
49. Müller, F. S. et al. Autoantibodies against the chemokine receptor 3 predict cardiovascular risk. *Eur. Heart J.* **44**, 4935–4949 (2023).
50. Yue, X. et al. Autoantibodies against C5aR1, C3aR1, CXCR3, and CXCR4 are decreased in primary Sjogren's syndrome. *Mol. Immunol.* **131**, 112–120 (2021).
51. Schwab, J. M. et al. Lesional antibody synthesis and complement deposition associate with de novo antineuronal antibody synthesis after spinal cord injury. *Neurol. Neuroimmunol. Neuroinflammation* **10**, e200099 (2025).
52. Ho, D., Imai, K., King, G. & Stuart, E. A. MatchIt: nonparametric preprocessing for parametric causal inference. *J. Stat. Softw.* **42**, 1–28 (2011).
53. Khanna, D. et al. Standardization of the modified Rodnan skin score for use in clinical trials of systemic sclerosis. *J. Scleroderma Relat. Disord.* **2**, 11–18 (2017).
54. Love, M. I., Huber, W. & Anders, S. Moderated estimation of fold change and dispersion for RNA-seq data with DESeq2. *Genome Biol.* **15**, 550 (2014).
55. Dobin, A. et al. STAR: ultrafast universal RNA-seq aligner. *Bioinformatics* **29**, 15–21 (2013).
56. Ashburner, M. et al. Gene Ontology: tool for the unification of biology. *Nat. Genet.* **25**, 25–29 (2000).
57. Subramanian, A. et al. Gene set enrichment analysis: A knowledge-based approach for interpreting genome-wide expression profiles. *Proc. Natl Acad. Sci.* **102**, 15545–15550 (2005).
58. Krämer, A., Green, J., Pollard, J. Jr & Tugendreich, S. Causal analysis approaches in Ingenuity Pathway Analysis. *Bioinformatics* **30**, 523–530 (2014).
59. Chen, Y.-Y. et al. Investigation of the keratinocyte transcriptome altered in high-glucose environment: An in-vitro model system for precision medicine. *J. Dermatol. Sci.* **109**, 37–46 (2023).
60. Chen, Y.-Y., Huang, S.-M., Cheng, Y.-W., Hsu, Y.-L. & Lan, C.-C. E. High-glucose impact on UVB responses in human epidermal keratinocytes: Insights on diabetic skin's resistance to photocarcinogenesis. *Life Sci.* **357**, 123083 (2024).

Acknowledgements

We thank Ms. Maiko Enomoto and her colleagues for their secretarial work. We appreciate K. Yamaguchi, T. Okumura, C. Ono, A. Sato, A. Miya, R. Kumagai, and N. Goshima from ProteoBridge Corporation for preparing the WPAs. We also acknowledge R. Uchino, Y. Murakami, and H. Matsunaka from NOV Academic Research, TOKIWA Pharmaceuticals Co. Ltd. for providing technical assistance with autoantibody measurement. This work was supported by JSPS KAKENHI Grant Number 25K19589 and 25HP8021. Research funding was additionally provided by TOKIWA Pharmaceutical Co., Ltd. The DESIRES trial was funded by Japan Agency for Medical Research and Development (AMED) Grant Number JP19ek0109299 and Zenyaku Kogyo Co, Ltd, Japan. As the trial was an investigator-initiated clinical trial, the funders were not involved in any way in the designing, analysis, interpretation, or drafting of the study.

Author contributions

K.M.M. primarily engaged in autoantibody measurement, clinical data collection, data analysis, visualization, and writing the first draft of the manuscript. Y.Y.C. primarily engaged in animal experiments, transcriptomic analysis, and writing the subject part of the manuscript. K.I. participated in machine learning analysis. S.E. was primarily engaged in the management of SSc patients who participated in the DESIRES trial. H.K. and H.S. took part in the sample collection of SSc and was involved in revising the manuscript. A.K. and A.Y.-O. took part in the sample collection of SSc. C.C.L. and H.S.Y. supervised YY Chen. S Sato conceptualized and supervised the study.

Competing interests

The authors declare no competing interests.

Additional information

Supplementary information The online version contains supplementary material available at https://doi.org/10.1038/s41467-025-66974-4.

Correspondence and requests for materials should be addressed to Kazuki M. Matsuda or Shinichi Sato.

Peer review information *Nature Communications* thanks Vincent Sobanski and the other anonymous reviewer(s) for their contribution to the peer review of this work. A peer review file is available.

Reprints and permissions information is available at http://www.nature.com/reprints